Journal of Ethnopharmacology 301 (2023) 115760

Contents lists available at ScienceDirect

Journal of Ethnopharmacology

journal homepage: www.elsevier.com/locate/jethpharm

Carob extract induces spermatogenesis in an infertile mouse model via upregulation of *Prm1*, *Plzf*, *Bcl-6b*, *Dazl*, *Ngn3*, *Stra8*, and *Smc1b*

Zeynab Ghorbaninejad [a,b,c], Atiyeh Eghbali [a,b,c], Mahsa Ghorbaninejad [a,d], Mahdi Ayyari [e], Jerzy Zuchowski [f], Mariusz Kowalczyk [f], Hossein Baharvand [a,b], Abdolhossein Shahverdi [c], Poopak Eftekhari-Yazdi [c,**], Fereshteh Esfandiari [a,*]

[a] Department of Stem Cells and Developmental Biology, Cell Science Research Center, Royan Institute for Stem Cell Biology and Technology, ACECR, Tehran, Iran
[b] Department of Developmental Biology, University of Science and Culture, Tehran, Iran
[c] Department of Embryology, Reproductive Biomedicine Research Center, Royan Institute for Reproductive Biomedicine, ACECR, Tehran, Iran
[d] Department of Genetics, Reproductive Biomedicine Research Center, Royan Institute for Reproductive Biomedicine, ACECR, Tehran, Iran
[e] Department of Horticultural Science, Tarbiat Modares University, Tehran, Iran
[f] Department of Biochemistry and Crop Quality, Institute of Soil Science and Plant Cultivation, State Research Institute, Puławy, Poland

ARTICLE INFO

Keywords:
Carob extract
Azoospermia
Spermatogenesis recovery

ABSTRACT

Ethnopharmacological relevance: Ethnopharmacological studies for drug discovery from natural compounds play an important role for developing current therapeutical platforms. Plants are a group of natural sources which have been served as the basis in the treatment of many diseases for centuries. In this regard, *Ceratonia siliqua* (carob) is one of the herbal medicine which is traditionally used for male infertility treatments. But so far the main mechanisms for effects of carob are unknown. Here, we intend to investigate the ability of carob extract to induce spermatogenesis in an azoospermia mouse model and determine the mechanisms that underlie its function.

Aim of the study: This is a pre-clinical animal model study to evaluate the effect of carob extract in spermatogenesis recovery.

Methods: We established an infertile mouse model with the intent to examine the ability of carob extract as a potential herbal medicine for restoration of male fertility. Sperm parameters, as well as gene expression dynamics and levels of spermatogenesis hormones, were evaluated 35 days after carob administration.

Results: Significant enhanced sperm parameters ($P < 0.05$) showed that the carob extract could induce spermatogenesis in the infertile mouse model. Our data suggested an anti-apototic and inducer role in the expressions of cell cycle regulating genes. Carob extract improved the spermatogenesis niche by considerable affecting Sertoli and Leydig cells ($P < 0.05$). The carob-treated mice were fertile and contributed to healthy offspring that matured. Our data confirmed that this extract triggered the hormonal system, the spermatogenesis-related gene expression network, and signaling pathways to induce and promote sperm production with notable level ($P < 0.05$). We found that the aqueous extract consisted of a polar and mainly well water-soluble substance. Carob extract might upregulate spermatogenesis hormones via its amino acid components, which were detected in the extract by liquid chromatography-mass spectrometry (LC-MS).

Conclusion: Our results strongly suggest that carob extract might be a promising future treatment option for male infertility. This finding could pave the way for clinical trials in infertile men. This is the first study that has provided reliable, strong pre-clinical evidence for carob extract as an effective candidate for fertility recovery in cancer-related azoospermia.

* Corresponding author. Department of Stem Cells and Developmental Biology, Cell Science Research Center, Royan Institute for Stem Cell Biology and Technology, ACECR, P.O. Box 16635-148, 1665659911, Tehran, Iran.
** Corresponding author. Department of Embryology, Reproductive Biomedicine Research Center, Royan Institute for Reproductive Biomedicine, ACECR, P.O. Box 16635-148, Tehran, 1665659911, Iran.
E-mail addresses: eftekhari@royaninstitute.org (P. Eftekhari-Yazdi), fereshtehesfandiari@royaninstitute.org (F. Esfandiari).

https://doi.org/10.1016/j.jep.2022.115760
Received 12 December 2021; Received in revised form 20 September 2022; Accepted 22 September 2022
Available online 6 October 2022

1. Introduction

Male infertility has various causes, including disruptions to the spermatogenesis process (Babakhanzadeh et al., 2020). Azoospermia is the most severe type of male infertility, and it affects 10%–20% of patients (Baker and Sabanegh Jr, 2013; Kumar, 2013). Current therapies for azoospermia include surgery techniques for sperm retrieval from the testis combined with intracytoplasmic sperm injection (ICSI) (Esteves et al., 2013). However, these techniques cannot successfully retrieve sperm in 50% of patients. Notably, the female partners of patients successfully treated by surgical means must receive hormonal therapy to become pregnant following ICSI.

Drug and hormonal therapies for azoospermia have serious adverse effects, including erectile dysfunction and mild loss of libido (Hu et al., 2018). Cardiovascular events and acceleration of prostate cancer growth (if cancer is already present) during the treatment period are adverse effects of anti-estrogen drugs such as clomifene citrate and tamoxifen, which are prescribed for azoospermic patients (Isidori et al., 2017). Therefore, it is of utmost importance to develop medications that lack adverse effects and can induce spermatogenesis in azoospermic patients and needless to use ICSI.

In this regard, Ethnopharmacology studies provides a platform for drug discovery from natural sources including plants (Sharma, 2017; Süntar, 2019). Herbal components appear to be promising alternatives to pharmaceuticals because these phytotherapeutic agents have fewer adverse effects compared to synthetic drugs. Although carob is traditionally used for male infertility (Faramarzi et al., 2019; Sharma, 2017), there is no adequate scientific basis to justify its use in the clinic. The mechanisms that underlies its function are unknown. Here, we intend to investigate the ability of carob extract to induce spermatogenesis in an azoospermic mouse model and determine the mechanisms that underlie its function. We also performed metabolite profiling of the carob extract that induced spermatogenesis in this azoospermia mouse model.

List of abbreviations

Bax	BCL2-associated X
Bcl-6b	B-cell CLL/lymphoma 6-member B protein
BMP4	Bone morphogenetic protein 4
cAMP	Cyclic adenosine monophosphate
Ccnd1	Cyclin D1
Cdk2	Cyclin dependent kinase 2
Cdk4	Cyclin dependent kinase 4
Cdk6	Cyclin dependent kinase 6
Cdc25a	Cell division cycle 25A
c-Kit	KIT proto-oncogene, receptor tyrosine kinase
c-Myc	MYC proto-oncogene, bHLH transcription factor
Dazl	Deleted in azoospermia-like
Etv-5	ETS variant transcription factor 5
Gapdh	Glyceraldehyde 3-phosphate dehydrogenase
GDNF	Glial cell-derived neurotrophic factor
Gfr-α1	GDNF family receptor alpha 1
ICSI	Intracytoplasmic sperm injection
ID1-1	Inhibitor of DNA binding 1
ID2	Inhibitor of DNA binding 2
Ki67	Marker of proliferation Ki-67
LH	Luteinizing hormone
Lhx1	LIM homeobox 1
Ngn3	Neurogenin 3
Pcna	Proliferating cell nuclear antigen
PGE2	Prostaglandin E2
Plzf	Promyelocytic leukemia zinc finger
Prm1	Protamine 1
P21	Cyclin dependent kinase inhibitor 1A
P57	Cyclin dependent kinase inhibitor 1C
ROS	Reactive oxygen species
Smc1b	Structural maintenance of chromosomes 1B
Smad1	SMAD family member 1
Smad2	SMAD family member 2
Smad3	SMAD family member 3
Smad5	SMAD family member 5
Smad7	SMAD family member 7
SOX9	SRY-box transcription factor 9
SSC	Spermatogonial stem cell
Stra8	Stimulated by retinoic acid 8
TGF-β:	Transforming growth factor β
Tnp1	Transition protein 1
Tnp2	Transition protein 2
Utf-1	Undifferentiated embryonic cell transcription factor 1
UHPLC-MS	Ultra-high performance liquid chromatography mass spectrometry
RP-UHPLC	Reversed phase ultra-high performance liquid chromatographic

2. Materials and methods

2.1. Plant material

Carob has distinguishing characteristics that are not confused with other species. Carob pods are quite special from the genus *Ceratonia*. Even other species of this genus do not have carob-like pods (*Ceratonia siliqua*). We bought these pods from a reputable herbal store. The pods of dried carob (*Ceratonia siliqua*), which is a well-known medicinal plant (GRUNER, 1930; MH, 1844; Stansbury, 2019), were purchased from a reputable herbal store and identified by Dr. Ayyari, Department of Horticultural Science, Faculty of Agriculture, Tarbiat Modares University in Tehran, Iran. The dried pods were subsequently ground into a powder prior to extraction.

2.2. Extraction

The carob extract was prepared according to traditional recipe (advised by herbal stores in Iran which is the same instruction used by infertile patients) and literature (Ata et al., 2018; Vafaei et al., 2018) with some modification. In this study, 120 g of carob powder was added in 1 L of boiling distilled water for 5 min, followed by filtration through no. 1 Whatman filter. Then, this extract was concentrated at 45 °C in a rotary evaporator and finally freeze dried into a powder.

Also, we prepared the hydroalcoholic carob extract as follows: 10 g of carob pods was extracted with sonication for 30 min with 70% ethanol/water (100 ml). The extract was filtered through a no. 1 Whatman paper, concentrated at 40 °C in a rotary evaporator, and finally freeze dried to remove the water residue. The hydroalcoholic carob extract powder was stored at −20 °C until analysis.

2.3. Chemicals

Formic acid (liquid chromatography-mass spectrometry [LC-MS]), acetonitrile (LC-MS grade), and isocratic grade methanol (MeOH) were obtained from Merck.

2.4. High-resolution liquid chromatography-mass spectrometry (LC-MS) analysis of the aqueous extract

The crude aqueous extract of the carob pods was dissolved in 5% methanol (~63 mg ml^{-1}), centrifuged (16 000×*g*, 10 min), and subjected to UHPLC-MS analysis. The compounds of the extract were determined by using a Thermo Ultimate 3000RS chromatographic system (Thermo Fisher Scientific, Waltham, MA, USA) equipped with a diode array detector (DAD), a charged aerosol detector (CAD), and coupled with a Bruker Impact II quadrupole time-of- flight (Q-TOF) mass spectrometer (Bruker Daltonik GmbH, Bremen, Germany). The extract was separated on a CORTECS T3 column (2.1 × 150 mm, 2.7 μm; Waters, Milford, MA, USA) and kept at 40 °C. The mobile phase A included 0.1% (v/v) formic acid in MilliQ water and mobile phase B consisted of acetonitrile that contained 0.1% (v/v) formic acid. The injection volume was 5 μL. Chromatographic elution was performed using a 20-min concave-shaped gradient from 1% to 70% of phase B. The total time of the chromatographic method was 25 min, and the flow rate was 0.500 ml min^{-1}.

Mass analyses were carried out using an electrospray ion source in the negative and positive ion modes. Negative ion analysis was accompanied by a CAD; the column effluent was diverted with a flow splitter in a 1:3 proportion between the parallel connected MS and CAD detector attached in. Positive ion measurements were combined with a diode array detection (200–600 nm). The MS scanning ranged from 100 to 2000 *m/z*. Subsequently, the following MS settings were used: capillary voltage 3 kV (negative ion mode) or 4 kV (positive ion mode), dry gas flow of 6 L min^{-1}, dry gas temperature of 200 °C, 0.7 Bar nebulizer pressure, collision RF 750 Vpp, 100 μs transfer time, and 10 μs prepulse storage. In each scan, two precursor ions with intensities that exceeded 2000 counts were fragmented. The collision energy was automatically set and depended on the *m/z* value of a fragmented ion, which ranged from 2.5 to 80 eV for the negative ion mode and from 1.25 to 50 eV for the positive ion mode. The obtained data were calibrated internally with a solution of sodium formate, which was introduced to the ion source via a 20 μL loop at the beginning of each separation. Constituents of the carob extract were tentatively identified on the basis of their MS, MS2, and UV spectra and a literature search of the data.

2.5. Animals

Adult male Naval Medical Research Institute (NMRI) mice (age: 8–10 weeks; weight range: 25–39 g; Royan Institute, Tehran, Iran) were housed in the Royan Institute Animal Laboratory under standard conditions of 23 ± 2 °C and a 12-h light-dark cycle with free access to water and food.

2.6. Infertile mouse model

In order to optimize our animal model with a defined dose of drug capable of creating an azoospermia model with the least lethal effect on mice, we investigated three different doses of busulfan (40,45 and 50 mg/kg, #B2635, Sigma-Aldrich, Germany) that were injected as single intraperitoneal (IP) injection (n = 4) to create azoospermia model (the infertile mice model) (Chen et al., 2021; Ghasemi et al., 2009; Jung et al., 2015; Bucci and Meistrich, 1987).

After 30 days, these male mice were allowed to mate naturally with mature female mice for five days in order to remove any possible abnormal sperm produced after the busulfan injections. Then, the testes and tails of the epididymides were collected after 35 days (duration of spermatogenesis) for sperm count and histological assessment in each group. The optimum dose of busulfan was selected based on survival of the mice, sperm concentration, and testicular histological analysis that was used as the infertile model in the experimental groups.

2.7. Experimental groups

The animals were classified into four groups: intact (normal mice), vehicle (negative control; mice that have been injected with busulfan but did not did not receive carob extract. This group is infertile model without any treatment with carob extract), Clomiphene citrate (positive control), and carob extract. The intact group comprised normal mice that did not receive an injection or treatment. The infertile mouse model (vehicle) was injected with busulfan, (45 mg/kg) and they received either carob extract or no treatment. The positive control group received clomiphene citrate to stimulate spermatogenesis (clomifene, 25 mg/kg) after an IP injection of busulfan. We examined three doses of carob extract, which were selected according to a previous study which was conducted in rats; in this study, rats received 150, 300, and 600 mg/kg of carob hydroalcoholic extract (Mokhtari et al., 2012). Then we used a dose calculation table (Nair and Jacob, 2016) (Supplementary table 1) that allows for the conversion of a drug dose administered to rats into the related dose for being used in mice. Based on this table we should divide the carob doses (used for treating rat animals) by two to calculate the related doses in mice. Therefore, the related doses in mice would be 75, 150 and 300 mg/kg. Moreover, we evaluated 600 mg/kg dose because we observed a dose-depend effect for carob in our study. Mice were gavaged with carob extract every day for 35 days (since the duration of mouse spermatogenesis is 35 days (Cordeiro et al., 2021).).

According to the results of a study, 10 cc of carob (150 g of carob beans boiled in 500 ml of tap water) was given to New Zealand white male rabbits, as the treatment group. In this group, there were no toxicological effects observed in the livers or kidneys of the rabbits which can be used for human consumption. Therefore, we did not anticipate any toxicities for these doses of carob extract.

2.8. Epididymal sperm collection

Tails of the epididymides were dissected and placed in Eppendorf tubes that contained 1 ml pre-warmed T6 culture medium plus 10% bovine serum albumin (BSA) in order to release the spermatozoa into the medium. The samples were incubated at 37 °C for 30 min, and then sperm concentration and motility were assessed by computer-assisted sperm analysis (CASA) with Sperm Class Analyzer® software (SCA, version 6, Microptic Co., Spain) and a phase-contrast microscope (Eclipse E−200; Nikon Co., Tokyo, Japan). A video camera (Basler Vision, A312FC at 50 fps; Technology Co., Ahrensburg, Germany) was attached to the microscope to capture images visualized under 100x magnification.

2.9. Sperm viability test

We used eosin Y staining to analyze sperm cell viability. First, 10 μl of sperm were mixed with 5 μl of eosin Y (0.5% w/v; Merck Chemical Co., Darmstadt, Germany). After 1 min, the sperm cells were stained and we counted at least 200 cells with a phase contrast microscopy at 100 × magnification (Olympus CX21, Tokyo, Japan). The spermatozoa that stained pink were considered to be nonviable and the unstained spermatozoa were presumed to be viable (Molaie et al., 2019).

2.10. Sperm morphology

Sperm morphology was assessed with a SpermBlue® Kit (Microptic, Spain), which includes two steps: sperm cell fixation on a simple slide and cell staining.

First, sperm cell smears were prepared on a slide (15 μl). After drying, the slides were placed in a fixation solution for 15 min and then placed in the staining solution for 20 min. Subsequently, the slides were washed five times with distilled water. At least 200 cells were counted under a phase contrast microscope at 100 × magnification (Olympus CX21, Tokyo, Japan). Sperm morphology was evaluated by previously

reported criteria (Hosseinpour et al., 2014; Van der Horst and Maree, 2010).

2.11. Analysis of DNA fragmentation by the sperm halo test

We evaluated sperm head DNA fragmentation according to the new version of the SCD test or sperm halo with a Sperm DNA Fragmentation Assay Kit (SDFA; ACECR, Tehran, Iran) based on the manufacturer's protocols (Artimani et al., 2018; Ziarati et al., 2019). According to the literature, there are five patterns of SCD: 1. large halo around the head of the sperm cell whose thickness is equal to or higher than the diameter of the sperm head; 2. medium halo where the diameter is equal to the minor diameter of the core; 3. very small halo with a thickness less than one-third of the minor diameter of the head; 4. no halo; and 5. degraded sperm cells with irregular staining around the head. Nuclei without DNA fragmentation by releasing DNA loops, forms large halo. Therefore, those with medium and large halos were considered to be normal sperm with DNA integrity and no fragmentation. Abnormal sperm had either small or no halos and were degraded with evidence of DNA fragmentation (Fernández et al., 2005). A minimum of 100 spermatozoa per sample was evaluated by light microscopy at 100x magnification (Olympus CX21, Tokyo, Japan).

2.12. Fluorescent measurement of intracellular reactive oxygen species (ROS) levels in sperm cells

We used flow cytometry to determine the level of reactive oxygen species (ROS), H_2O_2 and $O_2^{\bullet-}$, in the sperm samples. A sperm permeable stain, 2′,7′-dichlorofluorescin diacetate (DCFH-DA; Sigma Chemical Co., Germany) was used to detect intracellular H_2O_2, which is a stable and non-fluorescent probe. Dihydroethidium (DHE; Sigma Chemical Co., Germany) was used to detect intracellular $O_2^{\bullet-}$ (Ghaleno et al., 2014).

2.13. Histological analysis

The testes were fixed in Bouin's solution for 2 h, then fixed overnight at 4 °C with 10% neutral buffered formalin. The testes tissues were subsequently embedded in paraffin blocks, sectioned with a microtome into 6-μm thick slices, and placed on histological slides. We obtained 10 slides for each group that were stained with hematoxylin and eosin (H&E, Sigma-Aldrich) according to the standard protocols for light microscopic evaluation. We counted 10–14 cross-sections in each group.

2.14. Quantitative histological grading system

Johnsen's scoring was used to evaluate the level of sperm maturation and the quality of the spermatogenesis process (Curtis and Amann, 1981). We analyzed 10 sections in 10 slides for each group. Each section was counted and scored in five fields for the 20 seminiferous tubules. The number of tubules in each score was calculated as the percentage for each section. Mean data were obtained for each group. We scored the seminiferous tubules from 1 to 10 level based on the Johnsen's score, which the spermatogenic level was classified as Sertoli cell-only (SCO), spermatogonia arrest, spermatocyte arrest, spermatid maturation arrest, hypospermatogenesis, and normal spermatogenesis. The grading standard (Zhu et al., 2015) which we used in our study is presented in Fig. S7.

2.15. Gene expression analysis using quantitative real-time PCR

Total RNA was extracted from the whole testis using TRIzol reagent (Takara, #9108, Tokyo, Japan). The isolated RNA was reverse transcribed into cDNA using a PrimeScript 1st Strand cDNA Synthesis Kit (Takara, #6130, Tokyo, Japan) based on the manufacturer's instructions. Quantitative real-time PCR (qRT-PCR) was performed by using SYBR® Green Premix Ex Taq™ II (Tli RNase H Plus, Takara, #RR820L, Tokyo, Japan) in an ABI StepOne Plus™ thermocycler (Applied Biosystems, USA). The specificity of each primer pair was confirmed by melting curve analysis and agarose gel electrophoresis. The relative mRNA levels of the genes were evaluated by the $2^{-\Delta\Delta Ct}$ quantitative method and normalized to the housekeeping gene, glyceraldehyde 3-phosphate dehydrogenase (*Gapdh*). The experimental groups were analyzed in triplicate, and the results are presented as mean ± SEM. Supplementary Table 5 lists the primers and sequences.

2.16. Hormonal analysis

Serum samples were obtained from the hearts of the mice for hormonal analysis. The serum was isolated at 2500 rpm by centrifugation for 15 min. Then, the serum levels of testosterone and estradiol were measured by a kit (Bioassay Technology Laboratory, Shanghai, China; product code: E0260Mo and E0072Mo) and read with an ELISA reader.

2.17. Statistical analysis

GraphPad Prism 6 software was used to analyze all of the data. The results are expressed as mean ± SD. Statistical significance was done by one-way ANOVA and the post-hoc Fisher's LSD test, which was used to compare multiple significant differences between the groups. P-values <0.05 indicated statistical significance.

3. Results

3.1. Carob extract profile

A final brownish powder from the carob pod aqueous extract was obtained after freeze drying, and the yield of the aqueous extract was 9.37%. As expected, the aqueous extract consisted of a polar and mainly well water-soluble substance. The peaks were mostly composed of carbohydrates and some organic acids. These compounds, as well as diverse ester derivatives of disaccharides, were present in the extract. The first three chromatographic peaks consisted of a dihexose(s), a hexose(s), trisaccharides, organic acids, and other highly polar compounds and comprised about 74% of the total CAD peak area (Table 1, Fig. 1). Carob pods have a high source of sucrose and significant amounts of glucose and fructose. Thus, the detected di- and monosaccharides were most probably these three compounds (Deans et al., 2018). Interestingly, the extract also contained a significant number of dihexose derivatives, acylated with short-chain aliphatic acids (Table 1). Among these, compounds with the molecular formula $C_{16}H_{28}O_{12}$ were dominant. These compounds were probably dihexose isobutyrates since carob pods are known to have a high content of isobutyric acid (Berna et al., 1997).

Phenolic compounds consisted of diverse gallotannins, ellagic acid, and flavonoids (Table 1). The gallotannins were mainly different mono-, di-, and trigalloyl hexose isomers, and a tetragalloyl hexose was the dominant compound of this group. We also observed small amounts of gallic acid, dihexosides and siliquapyranone (or its isomer). The latter compound is a derivative of 2,3-digalloylglucose and (4R,6R)-4-hydroxy-6-methyl-tetrahydropyran-2-one, which was previously isolated from carob leaves (Deans et al., 2018). Flavonoids mostly included quercetin, myricetin, isorhamnetin and kaempferol/luteolin monoglycosides, though an apigenin *C*-hexoside-*C*-pentoside was also present. Quercetin 3-*O*-deoxyhexoside was the dominant flavonoid of the carob extract. This extract also contained an abundance of high polar constituents with sugar, amino acids, and simple organic acid derivatives.

3.2. Establishment of the infertile mouse model by busulfan injection, as an alkylating agent

Busulfan decreased the sperm count in a dose-dependent manner, with the most effective response at 50 mg/kg (Fig. S1A). However, there

Table 1
UHPLC-CAD-MS/MS analysis of the water extract of carob (*Ceratonia siliqua*) pods, the negative ion mode and reverse phase chromatography. The relative peak area is expressed as a percentage of the total area of all Charged Aerosol Detector (CAD) peaks.

No.	RT [min]	peak area fraction (%)	λ_{max} (nm)	parent ion (*m/z*)	fragment ions (*m/z*)	formula	error (ppm)	mSigma	tentative identification	Ref.
1	0.91	18.78		179.0561		$C_6H_{12}O_6$	0.2	9.8	hexose	(1–3)
				195.0510	177.0417 (3), 159.0276 (2), 129.0181 (7)	$C_6H_{12}O_7$	0.1	5.9	unidentified	
				209.0302	191.0195 (74), 173.0088 (8), 165.0401 (2), 147.0297 (15), 133.0145 (27), 129.0196 (13)	$C_6H_{10}O_8$	0.2	5.0	unidentified	
2	0.97	47.08		341.1092	179.0558 (100), 161.0454 (38), 149.0455 (17), 143.0341 (11), 131.0337 (9), 119.0345 (53)	$C_{12}H_{22}O_{11}$	−0.8	6.5	dihexose (sucrose ?)	(1–3)
				133.0128	115.0025 (68)	$C_4H_6O_5$	10.9	2.3	malic acid/isomer	
3	1.25	8.13		549.1670*	503.1625 (100), 341.1092 (72), 323.0986 (39), 221.0662 (18), 179.0559 (46), 161.0447 (10)	$C_{18}H_{32}O_{16}$	0.5	4.5	trihexose	
				519.1563*	473.1508 (100), 341.1087 (81), 323.0976 (11), 179.0563 (8), 161.0453 (24), 149.0443 (12)	$C_{17}H_{30}O_{15}$	0.7	5.0	dihexose-pentoside	
				191.0197	173.0092 (11), 147.0265 (3), 129.0180 (7), 111.0072 (36)	$C_6H_8O_7$	−0.1	2.7	(iso)citric acid/isomer	
				235.0464	217.0351 (80), 199.0244 (100), 155.0346 (31)	$C_8H_{12}O_8$	−1.9	5.2	unidentified	
				278.1244	235.0251 (31), 188.0926 (100), 158.0824 (10), 116.0709 (86)	$C_{11}H_{21}NO_7$	0.6	5.3	valine-hexose/isomer	
				290.0883	200.0568 (100), 128.0359 (37)	$C_{11}H_{17}NO_8$	−0.7	3.9	unidentified hexoside	
4	1.90	0.45		410.1665	188.0942 (25), 116.0709 (100)	$C_{16}H_{29}NO_{11}$	0.8	3.1	valine derivative	
				180.0669	163.0395 (33), 119.0471 (5)	$C_9H_{11}NO_3$	−1.4	2.6	tyrosine	
5	1.98	1.41	270	331.0677	271.0471 (8), 211.0249 (45), 169.0135 (26)	$C_{13}H_{16}O_{10}$	−1.9	14.8	gallic acid-hexose	(1)
				342.1197	180.0666 (100)	$C_{15}H_{21}NO_8$	−0.6	11.9	tyrosine-hexose	
				422.1306	254.0668 (14), 230.0687 (12), 200.0564 (100), 170.0449 (10), 154.0494 (6), 128.0339 (37)	$C_{16}H_{25}NO_{12}$/ $C_{17}H_{21}N_5O_8$	−0.6/ 2.6	6.0/8.2	unidentified	
				260.0236	216.0326 (30), 144.0111 (12), 112.0405 (7)				unidentified	
				159.0294	115.0388 (100)	$C_6H_8O_5$	3.2	7.0	unidentified acid	
6	2.41	0.86		429.1254*	383.1201 (43), 341.1096 (100), 323.0993 (30), 179.0559 (18)	$C_{14}H_{24}O_{12}$	−0.9	8.4	dihexose acetate	
				292.1401	202.1104 (18), 172.0982 (9), 130.0861 (100)	$C_{12}H_{23}NO_7$	0.1	9.2	(iso)leucine-hexose/ isomer	
7	2.51	1.43	270	169.0142	125.0239 (44)	$C_7H_6O_5$	0.4	6.1	gallic acid	
				302.0885	212.0567 (100), 140.0345 (68)	$C_{12}H_{17}NO_8$	−1.3	6.7	unidentified hexoside	
8	2.75	0.24		429.1256*	383.1200 (46), 341.1093 (100), 323.0986 (32), 221.0678 (4), 179.0569 (9), 161.0454 (7)	$C_{14}H_{24}O_{12}$	−1.5	5.0	dihexose acetate	
9	2.85	0.06		282.0843	150.0418 (50)	$C_{10}H_{13}N_5O_5$	0.4	10.6	guanosine	
			270	331.0673	271.0458 (100), 211.0248 (26), 169.0144 (10)	$C_{13}H_{16}O_{10}$	−0.5	0.6	gallic acid-hexose	(1)
10	3.11	0.36		304.1040	214.0723 (100), 184.0642 (14), 142.0495(45)	$C_{12}H_{19}NO_8$	−0.8	9.1	unidentified	
			275	483.0786	331.0669 (100), 313.0570 (82), 169.0139 (88), 125.0229 (13)	$C_{20}H_{20}O_{14}$	−1.3	4.2	digalloylhexose	(1, 4–6)
11	3.31	1.01		457.1564*	411.1512 (12), 342.1093 (100), 323.0983 (65), 179.0568 (12)	$C_{16}H_{28}O_{12}$	−0.3	6.6	(iso)butyryl dihexose	(1)
				424.1828	202.1086 (24), 130.0856 (100)	$C_{17}H_{31}NO_{11}$	−0.9	10.9	unidentified	
				436.1463	244.0826 (10), 226.0726 (7), 214.0722 (100), 184.0618 (11), 142.0495 (31)	$C_{17}H_{27}NO_{12}$	−0.6	18.0	unidentified	
12	3.47	0.06		326.1243	164.0717 (100)	$C_{15}H_{21}NO_7$	0.8	11.1	phenylalanine-hexose	
13	3.57	0.17	275	493.1203	331.0671 (11), 313.0566 (100), 283.0458 (43), 169.0138 (11)	$C_{19}H_{26}O_{15}$	−0.7	3.4	gallic acid dihexoside	(1, 5)
14	3.69	0.27		457.1562*	411.1501 (13), 341.1089 (100), 323.0984 (69), 179.0561 (11)	$C_{16}H_{28}O_{12}$	0.1	7.8	(iso)butyryl dihexose	(1)
			275	493.1202	331.0672 (23), 313.0565 (80), 271.0460 (100), 169.0138 (12)	$C_{19}H_{26}O_{15}$	−0.6	4.7	gallic acid dihexoside	(1, 5)
15	3.78	0.26		429.1614*	383.1565 (45), 293.0875 (2), 251.1136 (100), 233.0667 (4), 161.0442 (3)	$C_{15}H_{28}O_{11}$	−0.0	7.5	unidentified	
16	3.91	0.44		427.1462*	381.1406 (10), 293.0891 (25), 275.0770 (24), 249.0983 (22), 191.0563 (100), 149.0445 (77)	$C_{15}H_{26}O_{11}$	−1.0	4.6	(iso)butyryl-hexose-pentose	
17	3.98	0.38	275	483.0781	331.0668 (100), 313.0562 (68), 169.0141 (70)	$C_{20}H_{20}O_{14}$	−0.2	1.3	digalloylhexose	(1, 4–6)

(*continued on next page*)

Table 1 (*continued*)

No.	RT [min]	peak area fraction (%)	λ_{max} (nm)	parent ion (*m/z*)	fragment ions (*m/z*)	formula	error (ppm)	mSigma	tentative identification	Ref.
				305.0665	261.0758 (26), 219.9665 (20), 179.0354 (25), 165.0201 (17)	$C_{15}H_{14}O_7$	0.5	3.0	(epi)gallocatechin	(6)
18	4.30	0.69		457.1562*	411.1508 (14), 341.1090 (100), 323.0985 (88), 179.0563 (10)	$C_{16}H_{28}O_{12}$	0.2	7.3	(iso)butyryl dihexose	(1)
				427.1460*	293.0906 (14), 275.0788 (12), 191.0554 (100), 149.0446 (83)	$C_{15}H_{26}O_{11}$	−0.7	10.3	(iso)butyryl-hexose-pentose	(1)
19	4.43	0.43		763.2876**	293.0887 (100), 275.0780 (38), 221.0673 (18), 191.0547 (29), 149.0447 (36), 131.0338 (35)	$C_{15}H_{26}O_{11}$	0.1	8.8	(iso)butyryl-hexose-pentose	(1)
				461.1306	329.0879 (8), 167.0346 (100)	$C_{19}H_{26}O_{13}$	−1.1	17.4	vanillic acid-hexose-pentose	
20	4.57	0.62		427.1452*	381.1394 (3), 293.0876 (100), 233.0665 (22), 191.0559 (27), 149.0451 (13), 131.0337 (6)	$C_{15}H_{26}O_{11}$	0.9	1.7	(iso)butyryl-hexose-pentose	(1)
21	4.67	1.48		809.2925***	427.1456 (32), 381.1401 (65), 293.0878 (100)	$C_{15}H_{26}O_{11}$	0.9	14.2	(iso)butyryl-hexose-pentose	(1)
				158.0816	116.0706 (82)	$C_7H_{13}NO_3$	4.5	17.8	5-acetamidopentanoic acid/isomer	
22	4.80	0.88		411.1509	341.1082 (100), 323.0976 (27), 179.0573 (22)161.0453 (18)	$C_{16}H_{28}O_{12}$	−0.2	14.4	(iso)butyryl dihexose	(1)
23	4.91	2.29		457.1555*	411.1506 (100), 341.1089 (34), 323.0982 (73), 189.0770 (17), 179.0559 (6)	$C_{16}H_{28}O_{12}$	1.7	4.3	(iso)butyryl dihexose	(1)
				232.0827	214.0728 (36), 196.0615 (100)	$C_9H_{15}NO_6$	−0.3	16.0	unidentified	
24	5.01	2.25		457.1561*	411.1507 (85), 341.1092 (44), 323.0985 (100), 179.0560 (29)	$C_{16}H_{28}O_{12}$	0.3	4.3	(iso)butyryl dihexose	(1)
				212.0930	194.0809 (18), 168.1021 (33)	$C_{10}H_{15}NO_4$	−0.6	17.2	unidentified	
				175.0610	157.0500 (6), 131.0696 (3), 115.0384 (11)	$C_7H_{12}O_5$	0.9	5.7	unidentified carboxylic acid	
25	5.23	0.45		244.0280	200.0385 (40), 156.0481 (35), 128.0160 (9)				unidentified	
				457.1562*	411.1511 (4), 323.0981 (100). 203.0561 (5), 179.0561 (2)	$C_{16}H_{28}O_{12}$	0.2	4.8	(iso)butyryl dihexose	(1)
26	5.30	0.13		242.0667	198.0767 (60), 154.0861 (11)	$C_{10}H_{13}NO_6$	1.3	2.0	unidentified	
				483.0774	423.0581 (16), 331.0671 (18), 313.0563 (100), 271.0449 (73), 211.0239 (21), 169.0137 (56)	$C_{20}H_{20}O_{14}$	1.2	8.3	digalloylhexose	(1, 5, 6)
27	5.48	0.36		443.1920	237.1498 (2)	$C_{21}H_{32}O_{10}$	0.6	7.0	unidentified	
			270	305.0779	261.0871 (90), 189.0667 (100)	$C_{14}H_{14}N_2O_6$	0.1	7.8	unidentified	
28	5.57	0.74	275	483.0779	331.0666 (22), 313.0561 (46), 271.0455 (100), 241.0347 (6), 211.0243 (9), 169.0136 (15)	$C_{20}H_{20}O_{14}$	0.2	7.8	digalloylhexose	(1, 4–6)
				289.0712	245.0813 (70)	$C_{15}H_{14}O_6$	1.9	1.7	(epi)catechin	
29	5.84	0.51	270	635.0881	483.0754 (2), 465.0670 (22), 313.0562 (100), 169.0134 (27)	$C_{27}H_{24}O_{18}$	1.3	8.3	trigalloylhexose	(1, 4–6)
				441.1611*	395.1568 (8), 293.0883 (100), 233.0648 (46), 191.0566 (40), 149.0460 (16)	$C_{16}H_{28}O_{11}$	0.7	11.1	acylated hexose-pentose	
30	5.97	0.21		305.0775	261.0875 (100), 219.0772 (51), 201.0667 (55), 132.0442 (18), 116.0329 (34)	$C_{14}H_{14}N_2O_6$	1.3	4.9	unidentified	
				291.0142	247.0246 (100)	$C_{13}H_8O_8$	1.6	3.3	unidentified	
31	6.03	0.47		305.0774	261.0872 (100), 219.0775 (72), 201.0661 (68), 132.0435 (20), 116.0346 (17)	$C_{14}H_{14}N_2O_6$	1.5	15.4	unidentified	
32	6.20	0.10		461.1292*	415.1245 (9), 293.0882 (23), 191.0560 (16), 121.0285 (100)	$C_{18}H_{24}O_{11}$	1.9	1.9	acylated hexose-pentose	
33	6.24	0.22	275	595.1298	483.0777 (7), 443.1185 (100), 331.0665 (25), 313.0561 (14), 211.0253 (5), 169.0134 (65)	$C_{26}H_{28}O_{16}$	1.1	10.0	siliquapyranone/isomer	(1, 5, 7)
			275	635.0889	483.0782 (34), 465.0675 (97), 423.0557 (44), 313.0558 (100), 295.0453 (34), 169.0138 (42)	$C_{27}H_{24}O_{18}$	0.1	9.8	trigalloylhexose	(1, 4–6)
34	6.44	0.47		461.1288*	415.1206 (8), 293.0877 (16), 233.0678 (7), 191.0552 (15), 121.0286 (100)	$C_{18}H_{24}O_{11}$	2.7	11.5	acylated hexose-pentose	
				471.1717*	425.1653 (88), 341.1083(57), 323.0979 (100), 179.0550 (36), 161.0434 (16)	$C_{17}H_{30}O_{12}$	0.4	6.2	acylated dihexose	
35	6.59	0.15		485.1864*	341.1083 (100), 323.0987 (6), 179.0560 (10), 161.0456 (3)	$C_{18}H_{32}O_{12}$	2.5	6.4	(iso)capronyl dihexose	
				491.1404*	445.1346 (49), 323.0967 (99), 223.0600 (34), 121.0280 (100)	$C_{19}H_{26}O_{12}$	0.5	7.4	acylated dihexose	
36	6.74	0.40	275	635.0873		$C_{27}H_{24}O_{18}$	2.7	2.3	trigalloylhexose	

(*continued on next page*)

Table 1 (*continued*)

No.	RT [min]	peak area fraction (%)	λ_{max} (nm)	parent ion (*m/z*)	fragment ions (*m/z*)	formula	error (ppm)	mSigma	tentative identification	Ref.
					465.0664 (100), 313.0557 (75), 169.0131 (14)					(1, 4–6)
				431.1914*	385.1848 (100), 223.1347 (44), 205.1226 (75), 153.0903 (92)				unidentified	
37	6.90	0.24	275	317.0399$	465.0660 (14), 241.0351 (100), 169.0132 (31)	$C_{27}H_{24}O_{18}$	3.1	42.7	trigalloylhexose	(1, 4–6)
				172.0973	130.0854 (100)	$C_8H_{15}NO_3$	3.6	2.8	N-acetyl (izo)leucine	
				595.1304	483.0768 (71), 443.1198 (62), 389.1593 (61), 331.0678 (40), 313.0549 (67), 271.0447 (77), 169.0126 (33)	$C_{26}H_{28}O_{16}$	0.0	27.1	siliquapyranone/isomer	(1, 5, 7)
38	7.06	0.11	275	635.0871	483.0766 (69), 465.0667 (75), 313.0555 (51), 271.0451 (32), 221.0453 (22), 169.0135 (29)	$C_{27}H_{24}O_{18}$	2.2	5.1	trigalloylhexose	(1, 4–6)
39	7.34	0.06	275	635.0885	483.0777 (8), 465.0670 (100), 313.0568 (44), 169.0129 (13)	$C_{27}H_{24}O_{18}$	0.7	19.0	trigalloylhexose	(1, 4–6)
40	7.43	0.10		230.1029	212.0934 (13), 186.1133 (75), 168.1002 (9), 114.0922 (11)	$C_{10}H_{17}NO_5$	2.2	4.3	unidentified	
				527.1980	463.1834 (1), 383.1186 (6), 341.1086 (100), 323.0975 (12), 179.0557 (11)	$C_{21}H_{36}O_{15}$	0.2	12.6	acylated dihexose	
41	7.63	0.23	~270, 330	563.1397	473.1077 (47), 443.0970 (67), 383.0763 (59), 353.0658 (73)	$C_{26}H_{28}O_{14}$	1.7	17.7	apigenin C-hexoside-C-pentoside	(1, 5)
42	7.69	0.09	~260, 350	479.0823	316.0223 (100)	$C_{21}H_{20}O_{13}$	1.7	7.4	myricetin hexoside	(1, 4–6)
				186.1131	142.1224 (2), 116.0704 (3)	$C_9H_{17}NO_3$	2.3	0.6	unidentified	
43	8.11	1.21	280	787.0989	635.0884 (4), 465.0666 (100), 313.0559 (48), 295.0453 (16), 169.0136 (17)	$C_{34}H_{28}O_{22}$	1.3	6.8	tetragalloylhexose	(1, 4–6)
				485.1873*	439.1813 (21), 341.1082 (100), 323.0977 (35), 217.1076 (10), 179.0559 (12)	$C_{18}H_{32}O_{12}$	0.6	5.5	acylated dihexose	
44	8.35	0.56	255, 355	300.9987		$C_{14}H_6O_8$	1.1	2.5	ellagic acid	
				463.0873	316.0218 (100)	$C_{21}H_{20}O_{12}$	1.9	2.3	myricetin deoxyhexoside	(1, 4–6)
45	8.53	0.18		485.1871*	439.1819 (22), 341.1086 (100), 323.0976 (38), 179.0559 (22)	$C_{18}H_{32}O_{12}$	1.1	3.4	acylated dihexose	
46	8.61	0.09	255, 350	463.0874	300.0269 (100)	$C_{21}H_{20}O_{12}$	1.8	10.1	quercetin-3-O-hexoside	(1, 4–6)
47	8.89	0.05		433.0769	300.0271 (100)	$C_{20}H_{18}O_{11}$	1.6	6.0	quercetin-3-O-pentoside	(1, 4, 6)
48	9.04	0.06		433.0772	300.0267 (100)	$C_{20}H_{18}O_{11}$	1.1	5.0	quercetin-3-O-pentoside	(1, 4, 6)
49	9.44	1.07	255, 350	447.0929	300.0273 (100)	$C_{21}H_{20}O_{11}$	0.8	5.3	quercetin-3-O-deoxyhexoside	(1, 4–6)
				549.2546*	503.2506 (22), 371.2074 (100), 233.0651 (3), 161.0447 (5)	$C_{24}H_{40}O_{11}$	1.3	7.9	disaccharide derivative	
				187.0975	169.0856 12), 125.0958 (15)	$C_9H_{16}O_4$	0.2	2.9	unidentified	
50	9.98	0.08′		527.1976*	481.1923 (53), 411.1414 (55), 393.1394 (100), 341.1081 (16), 323.0960 (59), 249.0983 (28), 189.0765 (64)	$C_{20}H_{34}O_{13}$	1.0	13.4	di(iso)butyryl dihexose	
				200.1289	156.1395 (3), 130.0872 (9), 122.8727 (1)	$C_{10}H_{18}NO_3$	1.7	11.5	unidentified	
51	10.04	0.10		527.1979*	n.f.	$C_{20}H_{34}O_{13}$	0.4	4.3	di(iso)butyryl dihexose	
				511.2029*	465.1980 (20), 341.1095 (100), 323.0991 (46), 285.0400 (20), 179.0534 (24)	$C_{20}H_{34}O_{12}$	0.7	25.8	acylated dihexose	
52	10.20	0.07		447.0926	314.0428 (100)	$C_{21}H_{20}O_{11}$	1.5	16.8	isorhamnetin pentoside	
53	10.33	0.06		431.0978	284.0322 (100)	$C_{21}H_{20}O_{10}$	1.3	12.6	kaempferol/luteolin deoxyhexoside	
54	10.52	0.05		461.1087	314.0426 (100)	$C_{22}H_{22}O_{11}$	0.5	6.7	isorhamnetin deoxyhexoside	
				511.2030*	465.1935 (11), 341.1083 (100), 179.0549 (14)	$C_{20}H_{34}O_{12}$	0.5	24.1	acylated dihexose	
55	11.51	0.10		301.0356		$C_{15}H_{10}O_7$	−0.7	19.4	quercetin	(1, 4)
				285.0403		$C_{15}H_{10}O_6$	0.6	14.8	kaempferol/luteolin	(1, 4, 6)
				513.2184*	467.2126 (9), 341.1089 (100), 323.0979 (30), 185.1189 (19), 179.0565 (18), 143.1065 (30)	$C_{20}H_{36}O_{12}$	0.9	8.0	acylated dihexose	
56	11.89	0.08		557.2457*	383.1194 (7), 341.1087 (100), 323.0990)13), 179.0561 (11)	$C_{22}H_{40}O_{13}$	−1.0	12.9	acylated dihexose	

(*continued on next page*)

Table 1 (*continued*)

No.	RT [min]	peak area fraction (%)	λ_{max} (nm)	parent ion (*m/z*)	fragment ions (*m/z*)	formula	error (ppm)	mSigma	tentative identification	Ref.
57	13.35	0.12		327.2175	309.2076 (5), 291.1966 (5), 229.1444 (20), 211.1339 (17)	$C_{18}H_{32}O_5$	0.2	8.8	unidentified fatty acid	(1)
58	14.14	0.27		329.2334	311.2230 (2), 293.2109 (1), 229.1443 (16), 211.1336 (17), 171.1025 (4)	$C_{18}H_{34}O_5$	−0.3	4.5	unidentified fatty acid	
59	14.23	0.06		329.2332	311.2219 (3), 293.2120 (2), 229.1447 (17), 211.1343 (16), 171.1031 (4)	$C_{18}H_{34}O_5$	0.6	11.1	Unidentified1 fatty acid	

* formic acid (FA) adduct; ** $[2M-H]^-$; *** $[2M + FA-H]^-$; $ $[M-2H]^{2-}$; n.f. – not fragmented.
mSigma is a measure of a fit between the theoretical isotopic pattern for a proposed formula and the measurement results. The lower mSigma value, the better fit.

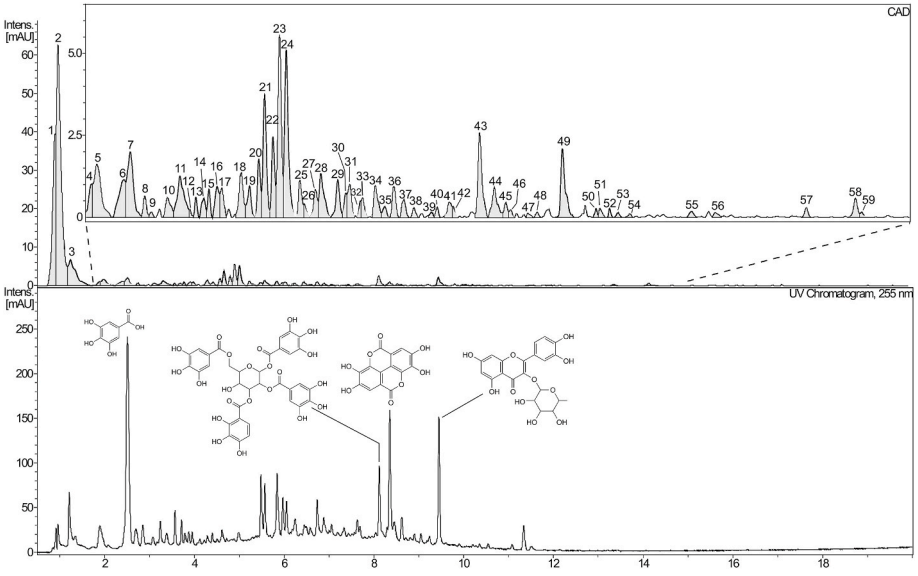

Fig. 1. RP-UHPLC chromatograms of carob pod water extract acquired by: (A) charged aerosol detector (CAD) and (B) diode array detector (DAD; λ = 255 nm). Structures of several identified compounds are shown. From left to right: gallic acid, a tetragalloylhexose (one of the possible structures), ellagic acid, and a quercetin 3-O-deoxyhexoside.

was a significant decrease in survival rate for 50 mg/kg compared to both the intact and lower doses of busulfan (Fig. S1B). Despite the more significant decrease of sperm count at 50 mg/kg, we omitted this dose from the study.

For further confirmation, we performed histological analysis of tissue from the mice that received the 40 and 45 mg/kg doses of busulfan. The results showed no significant changes in spermatogenesis in seminiferous tubules of mice injected with the 40 mg/kg of busulfan in comparison with the intact group, and the majority of tubules showed spermatogenesis. The 45 mg/kg dose impaired spermatogenesis, as shown by empty tubules with no spermatozoa or spermatogonia (Fig. S1C). In addition, the Johnsen score results showed that at 45 mg/kg of busulfan, 79% of seminiferous tubules had a score of 3, which indicated the presence of spermatogonia in tubules without spermatozoa or late spermatids. None of the seminiferous tubules had a score of 10, which indicated tubules with full spermatogenesis in the mice treated with busulfan (45 mg/kg). In the intact group, 79.3% of tubules had a Johnsen score of 10 (complete spermatogenesis). At the 40 mg/kg dose, 42.6% of tubules had a score of 3, and 10% of the tubules appeared to have complete spermatogenesis (Fig. S1D and Supplementary Table 2). Therefore, we selected the 45 mg/kg dose as the optimum dose of busulfan to use to produce the infertile mice model.

3.3. Carob administration induced spermatogenesis in the infertile mice model in a dose-dependent manner

In the vehicle group, there was a significant decrease in testicular weight ($P < 0.001$). Neither clomifene, nor administration of various doses of carob could increase testicular weight (Fig. S2).

CASA analysis results showed a notable, dose-dependent increase in sperm count following carob administration. The largest increase was observed with the 600 mg/kg dose ($P < 0.001$). Notably, the sperm counts in the group that received 600 mg/kg dose approximated those of the intact mice (Fig. 2A). Administration of 600 mg/kg of carob significantly increased total motility ($P < 0.01$) and progressive motility ($P < 0.05$) compared to the vehicle group (Fig. 2B and C). Also, mice treated with 300 and 600 mg of carob showed significant increase in terms of sperm count and total motility ($P < 0.05$) compared to positive control group (clomifene) (Fig. 2A and B).

Next, we investigated the additional insight into the effect of carob on sperm quality that SDFA results showed a considerable increase in DNA integrity in mice that received clomifene and all of the carob doses compared to the vehicle group (Fig. 2D). Consistently, DNA fragmentation significantly decreased in the same groups that had an increase in DNA integrity compared to the vehicle group (Fig. 2E).

Sperm viability analysis showed significant enhancement following treatment with 600 mg/kg of carob compared to the vehicle (Fig. 2F). Mice treated with 600 mg/kg of carob had increased sperm viability

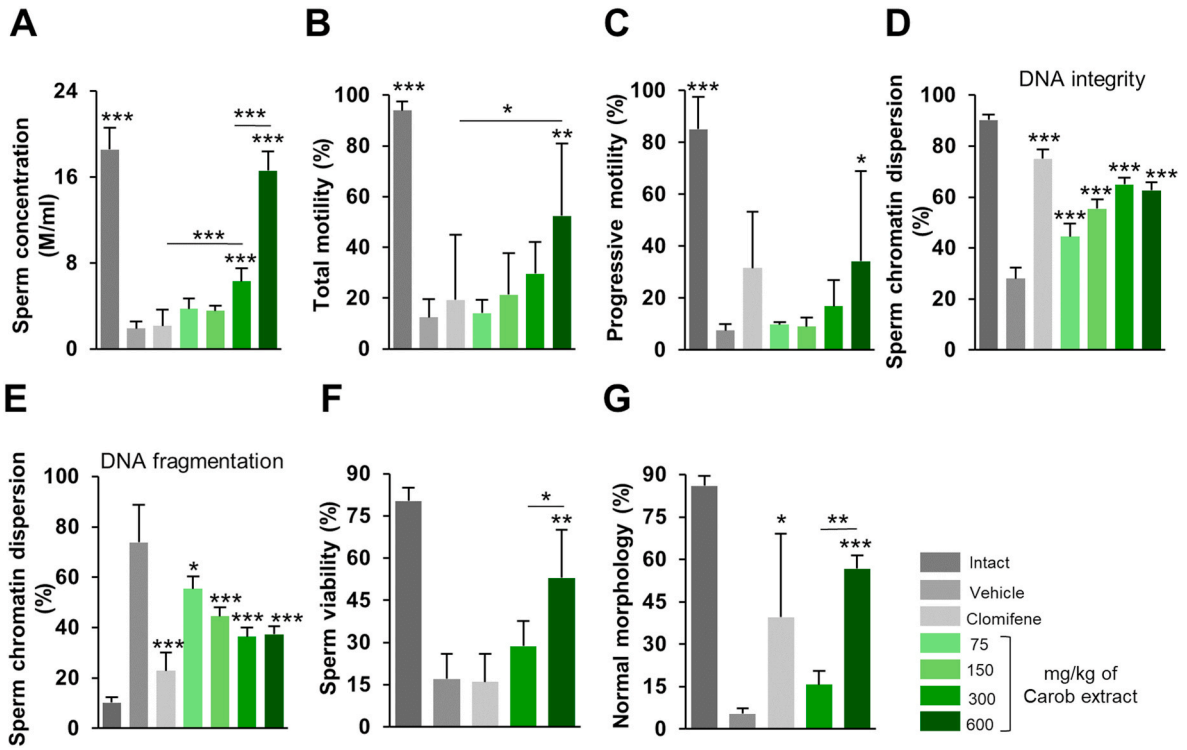

Fig. 2. Carob administration induced spermatogenesis in the infertile mouse model in a dose-dependent manner. (A) We assessed carob function in terms of sperm production. Sperm counts considerably increased in a dose-dependent manner after administration of carob. The most effective enhancement was seen at the 600 mg/kg dose. The 600 mg/kg and 300 mg/kg ($P < 0.001$) doses of carob increased sperm counts compared to the vehicle. There was a notable increase in the concentration of sperm after administration of 600 mg/kg of carob compared to 300 mg/kg of the extract ($P < 0.001$). (B–C) There were no significant increases in total and progressive motility in the carob-treated mice compared to the vehicle group, with the exception of the 600 mg/kg carob dose, which significantly increased total motility ($P < 0.01$) and progressive motility ($P < 0.05$) in comparison with the vehicle. (D) The DNA quality of the sperm showed that DNA integrity increased considerably in the mice in the carob groups and in the clomifene groups compared to the vehicle group ($P < 0.001$). (E) There was a significant decrease in DNA fragmentation in both carob groups and in the clomifene groups compared to the vehicle ($P < 0.05$). (F) There was significantly enhanced sperm viability compared to the vehicle after treatment with the 600 mg/kg dose of carob ($P < 0.01$). (G) The percentage of sperm with normal morphology at the 600 mg/kg dose of carob significantly increased in comparison with the vehicle ($P < 0.001$). There was a significantly increased percentage of sperm with normal morphology in the clomifene group compared to the vehicle group ($P < 0.05$).

compared to the group that received 300 mg/kg of the extract (Fig. 2F). The percentages of sperm with normal morphology at the 600 mg/kg carob dose significantly increased compared to the vehicle group and 300 mg/kg extract (Fig. 2G). Supplementary Fig. 4A shows criteria for recognizing sperms with normal morphology as well as abnormal morphology.

Our flow cytometry results showed significant decreases in both H_2O_2 and $O_2^{\cdot}$ as the most important intracellular ROS following carob administration in comparison with the vehicle group ($P < 0.05$) (Fig. 3A and B and Fig. S6).

To assess the spermatogenesis recovery following carob consumption, we evaluated the estradiol hormone. Our results showed a significant increase at 600 mg/kg of the carob extract in comparison with the vehicle group ($P < 0.05$). The level of estradiol in this group was notably

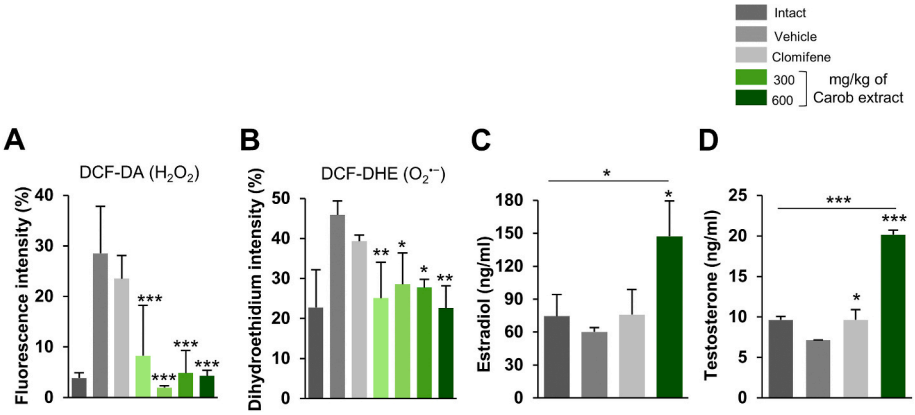

Fig. 3. Effect of carob administration on reactive oxygen species (ROS) and induction of hormonal axis in the infertile mouse model in a dose-dependent manner. (A–B) Reactive oxygen species (ROS) levels in sperm after carob treatment indicated that H_2O_2 was significantly decreased after carob administration compared to the vehicle group ($P < 0.001$) and there was a notable change in $O_2^{\cdot}$ levels following carob administration compared to the vehicle group ($P < 0.05$). (C–D) Hormonal analyses showed that estradiol hormone significantly increased after administration of the 600 mg/kg dose of carob in comparison with the vehicle group ($P < 0.05$). There was a remarkable increase in testosterone hormone secretion at the 600 mg/kg dose of carob in comparison with the vehicle group ($P < 0.001$). Data are shown for two to five independent experiments. Bars indicate mean ± SD. Based on assessment of the data distribution, statistical significance was tested by one-way ANOVA with post-hoc Fisher's LSD test. *$P \leq 0.05$, **$P \leq 0.01$, ***$P < 0.001$.

higher than the intact group ($P < 0.05$) (Fig. 3C). In addition, the serum level of testosterone following carob administration significantly increased in the 600 mg/kg carob group in comparison with the vehicle group ($P < 0.001$). Serum testosterone levels in the clomifene group were remarkably increased in comparison with the vehicle group ($P < 0.05$) (Fig. 3D).

3.4. Aqueous extract is the efficient method for extract preparation

We examined whether the method of extraction preparation could affect the ability of carob to induce spermatogenesis. We compared hydroalcoholic with the aqueous extract of carob at the 600 mg/kg concentration, which was the most efficient concentration for inducing spermatogenesis. The aqueous extract significantly increased sperm parameters in comparison with the vehicle group ($P < 0.05$) (Figs. S3A–C). However, the hydroalcoholic extract did not increase sperm parameters compared to the vehicle group (Figs. S3D–F). Since hydroalcoholic extract failed to induce spermatogenesis, therefore, we excluded this extract from the study and performed the rest of experiments on the aqueous extract.

3.5. Histological analysis revealed induced spermatogenesis following carob administration

Histological analysis of the seminiferous tubules showed that 300 mg/kg and, especially, 600 mg/kg of carob induced spermatogenesis in the infertile mice model, which was revealed by the presence of spermatogonia and sperm in the majority of tubules that were morphologically similar to the intact mice. Although we observed full spermatogenesis in a few tubules at the 75 and 150 mg/kg doses of carob, the majority of tubules were empty. Most tubules were empty in the vehicle group. There was a significant increase in the number of tubules with full spermatogenesis in the group that was gavaged with 600 mg/kg of carob in comparison with the vehicle (Fig. 4A).

We also performed quantitative histological evaluations for the 300 mg/kg and 600 mg/kg concentrations of carob because these two concentrations could effectively induce spermatogenesis. There was a notable increase in the number of tubules that had partial and full spermatogenesis, specially most of the tubules had completed the spermatogenesis process at the 600 mg/kg dose in comparison with the vehicle group ($P < 0.05$) (Fig. 4B, Supplementary Table 3), while in the vehicle group almost all tubes were empty with no spermatogenesis. In fact, this quantitative evaluation showed that nearly 80% of the vehicle group's tubules were empty spermatogenesis, and in this group, less than 5% of tubules contain full spermatogenesis. Instead, in the highest dose of the extract, i.e., 600 mg/kg, more than 60% of the tubules contain full spermatogenesis. In addition, histological grading based on Johnsen's score index (Fig. S7) revealed that at the 600 mg/kg carob dose, spermatogenesis was consistent with many elongated spermatids and an appropriate number of spermatozoa (scores 9 and 10) ($P < 0.01$) compared to the vehicle group that had spermatogonia with a small number of primary spermatocytes and no sperm (scores 3–4) ($P <$

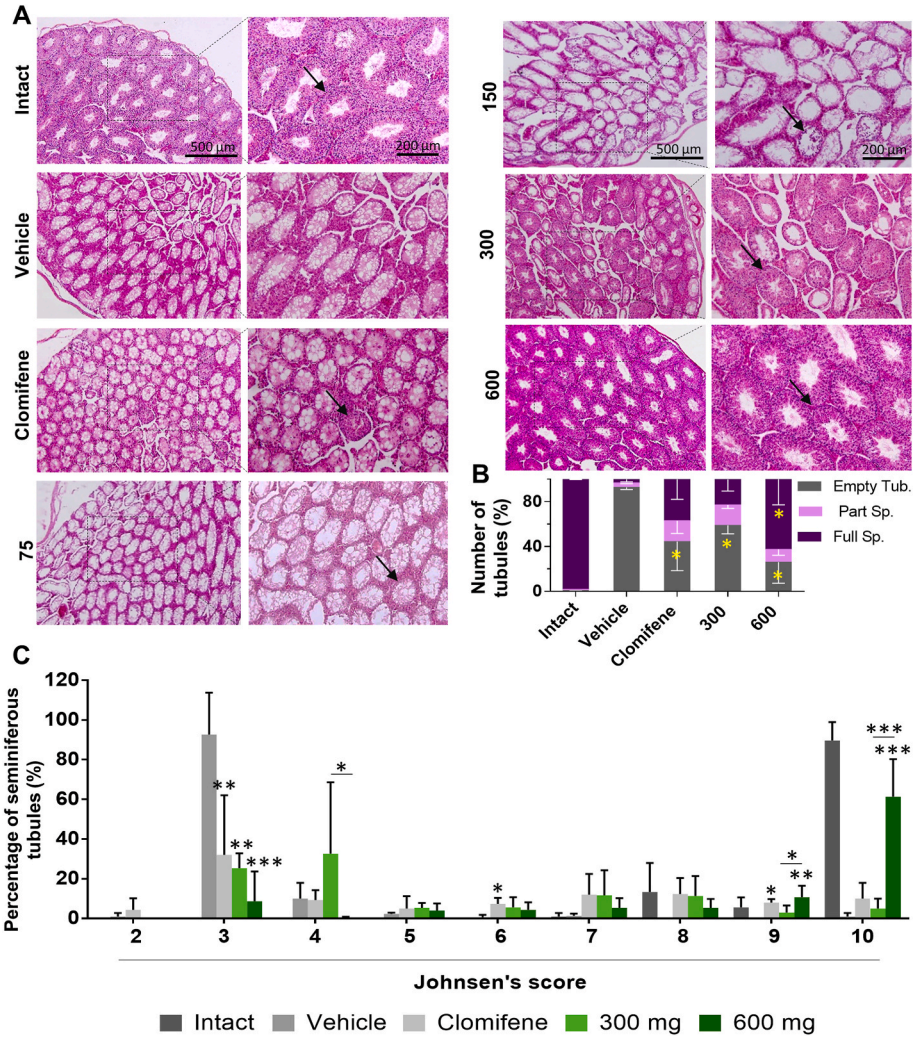

Fig. 4. Hematoxylin and eosin (H&E) evaluation of spermatogenesis following carob administration in the infertile mouse model. (A) Histological analysis showed that the 300 mg/kg dose induced spermatogenesis in the infertile mouse model as revealed by the presence of spermatogonia and sperm in the majority of tubules. Morphology of the seminiferous tubules after administration of 600 mg/kg carob was similar to intact mice (hematoxylin and eosin [H&E] staining). Red arrows show spermatogenesis in seminiferous tubules of the testes. Full spermatogenesis was observed after administration of carob extract, clomifene, and the intact groups. The majority of tubules were empty of spermatogonia and spermatozoa in the vehicle group. (B) There was a considerable increase ($P < 0.05$) in tubules that had partial and full spermatogenesis and a notable decrease in empty tubules after administration of 600 mg/kg carob in comparison with the vehicle group. Yellow stars show significant comparisons between the clomifene, 300 mg/kg carob, 600 mg/kg carob, and vehicle groups. (C) Johnsen's scores of 9 and 10 were noted at the 600 mg/kg carob dose. At this dose, we observed numerous elongated spermatids and an appropriate number of spermatozoa compared to the vehicle group, which had spermatogonia with a small number of primary spermatocytes (score 3–4) ($P < 0.001$). Data for three independent experiments. Bars indicate mean ± SD. Based on assessment of data distribution, statistical significance was tested by one-way ANOVA with post-hoc Fisher's LSD test. *$P \leq 0.05$, **$P \leq 0.01$, ***$P < 0.001$. (For interpretation of the references to colour in this figure legend, the reader is referred to the Web version of this article.)

0.001). At the 600 mg/kg carob dose, 61.33% of seminiferous tubules had a score of 10, or full spermatogenesis, compared to 89.66% in the intact group. We observed tubules full of spermatogonia and sperm in only 1% of the vehicle group. At the 300 mg/kg dose, 25.33% of the tubules had a score of 3, and 5% of tubules appeared to have complete spermatogenesis (Fig. 4C and Supplementary Table 4).

3.6. Gene expression pattern underlying carob treatment in mouse testes

We sought to determine the expression patterns of candidate genes that might activate upon carob administration. Both the 300 and 600 mg/kg extracts were included in the gene expression analysis to determine the mechanism by which 600 mg/kg of carob improved some of the sperm parameters compared to the 300 mg/kg extract.

As expected, our results indicated that 600 mg/kg of carob considerably elevated the levels of spermatogonial stem cell (SSC) self-renewal genes (*Plzf, Gfr-α1, Bcl-6b,* and *Utf-1*), along with SSC differentiation genes including: *Dazl, c-Kit, Ngn3, Stra8,* and *Smc1b* in comparison with the vehicle group ($P < 0.05$). Expressions of *Utf-1, Dazl, Ngn3,* and *Smc1b* significantly increased with the 600 mg/kg extract compared to the 300 mg/kg extract of carob ($P < 0.05$). *c-Kit* showed a reverse pattern ($P < 0.01$) (Fig. 5A and B). *Lhx-1,* as an SSC marker for self-renewal expressed in undifferentiated spermatogonia cells, significantly decreased in both the 300 and 600 mg/kg carob extract groups in comparison with the vehicle group ($P < 0.05$) (Fig. 5A).

We also evaluated *Prm1*, *Tnp1,* and *Tnp2* expressions following carob administration. There was a significant increase in *Prm1* expression with 600 mg/kg of carob ($P < 0.01$) and reduced expression of this gene with 300 mg/kg of carob ($P < 0.05$) in comparison with the vehicle group. *Prm1* expression remarkably increased in the 600 mg/kg group compared to the 300 mg/kg group ($P < 0.001$). Both *Tnp1* ($P < 0.01$) and *Tnp2* ($P < 0.05$) expressions significantly decreased in the 300 mg/kg carob group in comparison with the vehicle group, while their expressions increased significantly at the 600 mg/kg dose in comparison with both the vehicle and 300 mg/kg dose of the extract ($P < 0.005$) (Fig. 5C).

We also assessed the changes in expression of *Vimentin* and SRY-box transcription factor 9 (*Sox9*) (Sertoli cell-related genes) and *Nestin* (Leydig cell marker). Our results showed that the 600 mg/kg carob extract notably increased *Vimentin*, *Sox9*, and *Nestin* levels ($P < 0.05$). In comparison, the 300 mg/kg extract remarkably increased Sertoli cell-related gene expressions ($P < 0.05$), but not the Leydig cell marker compared to the vehicle. *Vimentin* expression significantly increased in the 300 mg/kg group in comparison with the 600 mg/kg group ($P < 0.01$), while *Nestin* showed an inverse expression pattern ($P < 0.05$) (Fig. 5D).

Ki67, as a marker for cell proliferation, was significantly increased in the 600 mg/kg group in comparison with the vehicle group ($P < 0.05$), but not in the 300 mg/kg group (Fig. 5E).

We analyzed the expression levels of BMP4 pathway components *Smad1/5*, *BMP4*, *Id1-1, Id1-2*, and *Id2* (Fig. 6A). Our results revealed that *Smad1*, *Smad5*, *BMP4*, *Id1-1*, and *Id2* expressions were significantly enhanced in both the 300 ($P < 0.05$) and 600 mg/kg ($P < 0.01$) concentrations of the carob extract in comparison with the vehicle group.

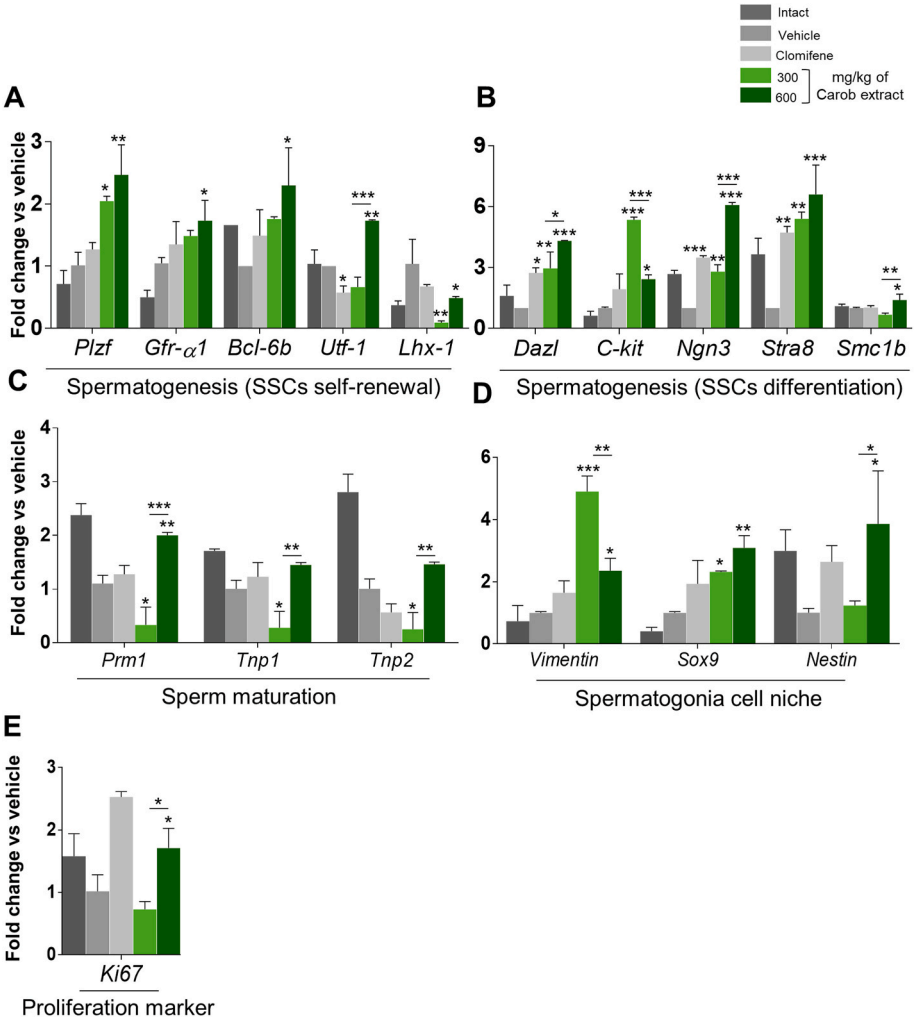

Fig. 5. Gene expression analysis following carob administration. (A–B) Gene expression analysis in mouse testes gavaged with the 600 mg/kg dose of carob showed elevated expressions of *Plzf*, *Gfr-α1*, *Bcl-6b,* and *Utf-1* as well as the spermatogonial stem cell (SSC) differentiation genes including: *Dazl, c-Kit, Ngn3, Stra8,* and *Smc1b* in comparison with the vehicle group ($P < 0.05$). *Lhx1,* a self-renewal SSCs marker, had significantly decreased expression in the groups that were treated with 300 mg/kg and 600 mg/kg carob in comparison with the vehicle group ($P < 0.05$). (C) Analyses of *Prm1*, *Tnp1,* and *Tnp2* revealed that *Prm1* expression significantly increased in the 600 mg/kg carob group ($P < 0.01$) and decreased in the 300 mg/kg carob group ($P < 0.01$) compared to the vehicle group. *Tnp1* and *Tnp2* expressions significantly increased at the 600 mg/kg dose in comparison with the vehicle group and 300 mg/kg dose ($P < 0.005$). (D) Also, 600 mg/kg of carob significantly increased expressions of *Vimentin*, *Sox9*, and *Nestin* (Sertoli cell-related and Leydig cell genes) ($P < 0.05$) in comparison with the vehicle group. (E) *Ki67,* an important gene in cell proliferation, significantly increased with the 600 mg/kg dose of carob in comparison with the vehicle group ($P < 0.05$). Data for three independent experiments. Bars indicate mean ± SD. Based on assessment of data distribution, statistical significance was tested by one-way ANOVA with post-hoc Fisher's LSD test, *$P \leq 0.05$, **$P \leq 0.01$, ***$P \leq 0.001$.

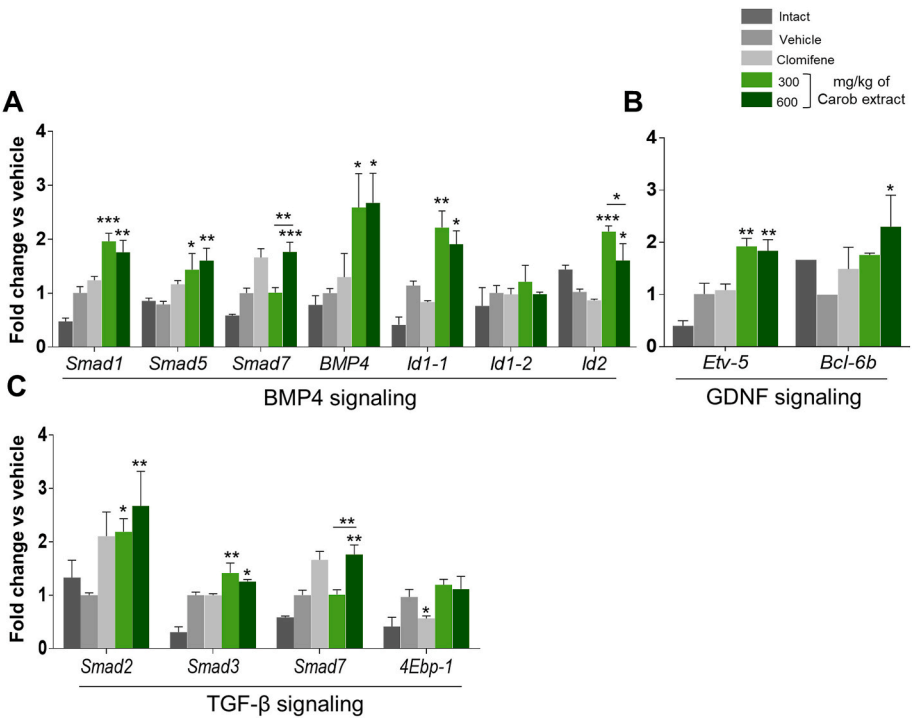

Fig. 6. Gene expression analysis of signaling pathway following carob administration. (A) Quantitative real-time PCR (qRT-PCR) analysis of genes associated with the major component of the BMP4 pathway revealed significant increases in *Smad1*, *Smad5*, *Bmp4*, *Id1-1,* and *Id2* expressions for both 300 mg/kg and 600 mg/kg ($P < 0.05$) groups of carob in comparison with the vehicle group. (B) GDNF target genes are involved in spermatogonial stem cell (SSC) self-renewal. *Etv-5* and *Bcl-6b* significantly increased with the 600 mg/kg carob group in comparison with the vehicle group ($P < 0.05$). (C) The downstream effectors of the transforming growth factor β (TGF-β) pathway showed that *Smad2*, *Smad3*, and *Smad7* levels significantly increased in the 600 mg/kg carob group in comparison with the vehicle group ($P < 0.01$). Data for three independent experiments. Bars indicate mean ± SD. Based on assessment of data distribution, statistical significance was tested by one-way ANOVA with post-hoc Fisher's LSD test, *$P \leq 0.05$, **$P \leq 0.01$, ***$P \leq 0.001$.

Id2 had significantly increased expression in the 600 mg/kg group in comparison with the 300 mg/kg group ($P \leq 0.01$). *Id1-2* showed no notable differences in the different experimental groups (Fig. 6A). The GDNF target genes were also upregulated in the carob-treated testes; *Etv-5* remarkably increased in both the 300 and 600 mg/kg carob extracts in comparison with the vehicle group ($P < 0.01$), and *Bcl-6b* increased significantly in the 600 mg/kg group, but not the 300 mg/kg group compared to the vehicle group ($P \leq 0.05$) (Fig. 6B).

No direct gene that targets spermatogenesis has been identified for the TGF-β signaling pathway. Therefore, we assessed the downstream effectors of these pathways (*Smad2*, *Smad3*, and *Smad7*). Both *Smad2* and *Smad3* levels significantly increased in the 300 ($P < 0.01$) and 600 mg/kg ($P < 0.005$) carob groups in comparison with the vehicle, whereas *Smad7* had a remarkable increase only in the 600 mg/kg carob group compared to both the vehicle and 300 mg/kg groups ($P \leq 0.01$) (Fig. 6C).

Our results showed that *Cdk4, Cdk6*, and *Ccnd1* expressions, as activators of the cell cycle, significantly increased in the 600 mg/kg group in comparison with the vehicle group ($P \leq 0.05$). *Cdk4, Cdc25a, Ccnd1*, and *c-Myc* expressions, as cell cycle activators, were remarkably decreased in the 600 mg/kg group compared to the 300 mg/kg carob group ($P \leq 0.05$). *Cdk4, Cdk6, Ccnd1*, and *c-Myc* had considerably

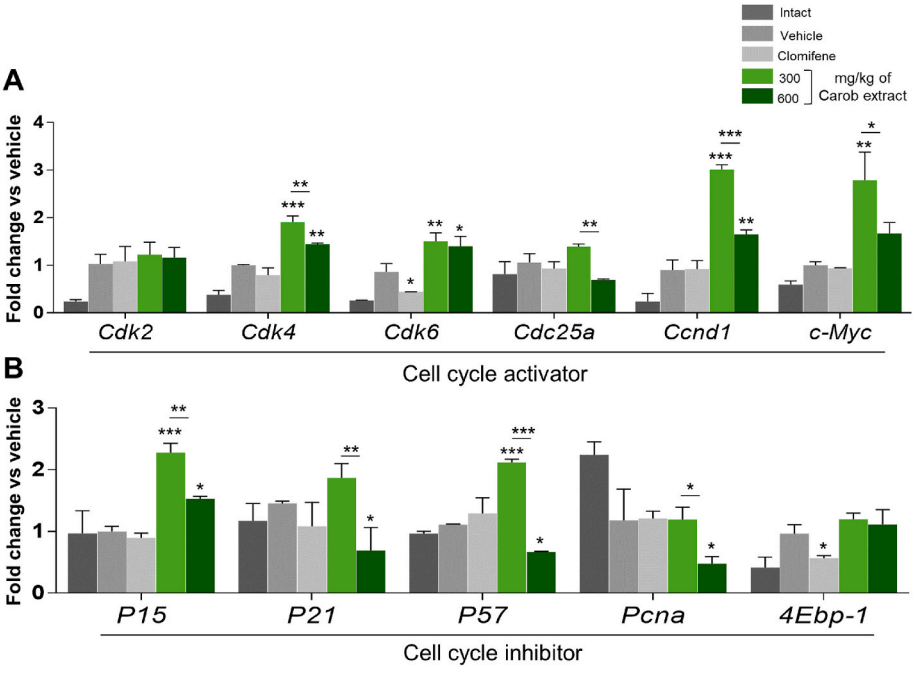

Fig. 7. Cell cycle-related genes expression analysis in testes of carob-treated mice. (A) Cell cycle related genes are essential factors for germ cell proliferation. Expression of *Cdk4, Cdk6,* and *Ccnd1*, as activators of the cell cycle, significantly increased with the 600 mg/kg dose in comparison with the vehicle group ($P \leq 0.01$). *Cdk2* expression showed no significant changes in the treated groups. (B) *P21*, *P57,* and *Pcna* expressions, as inhibitors of cell cycle genes, significantly decreased at the 600 mg/kg dose in comparison with the vehicle group ($P < 0.05$). However, *P15,* an inhibitor of the cell cycle, significantly increased at the 600 mg/kg dose in comparison with the vehicle group ($P < 0.05$). Data for three independent experiments. Bars indicate mean ± SD. Based on assessment of data distribution, statistical significance was tested by one-way ANOVA with post-hoc Fisher's LSD test. *$P \leq 0.05$, **$P \leq 0.01$, ***$P \leq 0.001$.

increased expressions after administration of 300 mg/kg of carob in comparison with the vehicle group ($P \leq 0.01$). *Cdk2* showed no significant changes in the treated groups (Fig. 7A). Inhibitors of the cell cycle genes, including *P21*, *P57*, and *Pcna* significantly decreased with 600 mg/kg of the extract in comparison with the vehicle group ($P < 0.05$). *P15*, a cell cycle inhibitor, was notably increased in the 600 mg/kg group in comparison with the vehicle group ($P < 0.05$). *P15, P21, P57*, and *Pcna* expression levels significantly decreased in the 600 mg/kg group in comparison with the 300 mg/kg group ($P < 0.01$), and the levels of *P15* and *P57* significantly increased in the 300 mg/kg group in comparison with the vehicle group ($P \leq 0.001$) (Fig. 7B).

Considering that busulfan can induce apoptosis, reproductive toxicity, and DNA damage, we sought to determine if the carob extract could improve the adverse effects of busulfan on the apoptosis process. Our results indicated that expressions of the pro-apoptotic components *Bax*, *Casp3*, and *P53* remarkably increased in the vehicle group in comparison with the intact group ($P < 0.05$). The anti-apoptotic gene, *Bcl-2* was considerably elevated in the 300 mg/kg and 600 mg/kg groups compared to the vehicle group ($P \leq 0.01$). *Bcl-2* expression was notably reduced in the 600 mg/kg group in comparison with the 300 mg/kg group ($P < 0.05$) (Fig. 8). As expected, the pro-apoptotic gene, *Bax*, was significantly decreased in both the 300 and 600 mg/kg groups in comparison with the vehicle group ($P < 0.05$), and there was a considerable decrease at the 600 mg/kg dose in comparison with 300 mg/kg of carob ($P \leq 0.05$). *Casp3* had significantly decreased expressions in the 300 mg/kg and 600 mg/kg doses of carob in comparison with the vehicle group ($P \leq 0.001$) (Fig. 8). There were no significant changes in *p53* expression in the treated groups in comparison with the vehicle.

3.7. Carob-treated mice were fertile and contributed to healthy, fertile offspring

Two out of four mice treated with 600 mg/kg carob, two mice were conceived (Fig. S4B and Supplementary Table 6). The male and female offspring from the carob-treated mice developed normally and grew into fertile adults, while in the vehicle group, only one out of 3 mice got pregnant. However, offspring derived from vehicle were infertile (Fig. S4C).

4. Discussion

The medicinal use of herbs has captivated the attention of experts for the treatment of reproductive disorder (Sharma et al., 2016) because of their decreased adverse effects compared to chemical drugs and their compatibility with human physiology (Hossen et al., 2016; Sharma et al., 2016).

Our findings of the carob ingredients including phenolics were consistent with the literature (Farag et al., 2019; Owis and El-Naggar, 2016; Papagiannopoulos et al., 2004). Additional phenolic compounds observed in the previously mentioned research could be attributed to extraction with some organic solvents, whereas in the current study we simulated the extraction based on a traditional remedy by decoction with water. A rich source of carbohydrates, some organic acids and amino acids, as well as diverse ester derivatives of disaccharides do not appear to be responsible for its bioactivity. In contrast, we observed small amounts of phenolic compounds that were mainly represented by gallotannins and simple flavonol glycosides. Although these phenolic compounds (especially flavonoids) often occur at significant levels in many different plants, they are not commonly found in plants that have fertility-stimulating properties. Thus, carob phenolics do not appear to be responsible for the activity of the extract. There were low detectable levels of nitrogen containing compounds, but most were tentatively identified as amino acids and amino acid glycosides. A number of compounds remained unidentified, and these might be potential candidates for active constituents of the extract (Table 1). However, it is possible that the active compounds belong to the most polar components of the carob pods and remain undetected due to ionization suppression effects caused by the presence of co-eluting organic acids and large amounts of carbohydrates. In addition, a type of synergism could be the main reason for this bioactivity and while a portion of the carbohydrates, amino acids, and phenolics could be responsible for the effect. Activity-guided isolation of active ingredients should be performed as the next step in future research on spermatogenesis-inducing compounds from carob pods.

Although Mokhtari et al. mentioned that precursor of prostaglandins including gamma-linolenic acids and alpha-linolenic acid and subsequently arachinonic acid, are responsible for inducing the secretion of sex hormones, but in our aqueous extract of carob which induces spermatogenesis, a trace amount of fatty acids were identified (Mokhtari et al., 2012). Our LC-MS data confirmed these various fatty acids and amino acids in carob extract.

We found that carob could serve as an effective factor to induce spermatogenesis in male infertility, as shown by the increase in sperm counts in an infertile mice model to its level in intact mice. Sperm motility, viability, and normal morphology significantly increased following carob administration. These parameters are crucial for successful fertilization (Henkel et al., 2005; Kovac et al., 2017; Zheng et al., 2016). Further, our study showed the strong positive effects of carob on active and complete spermatogenesis that is associated with mature spermatozoa as evidenced by Johnsen's score (Curtis and Amann, 1981). We observed complete spermatogenesis with spermatids and mature

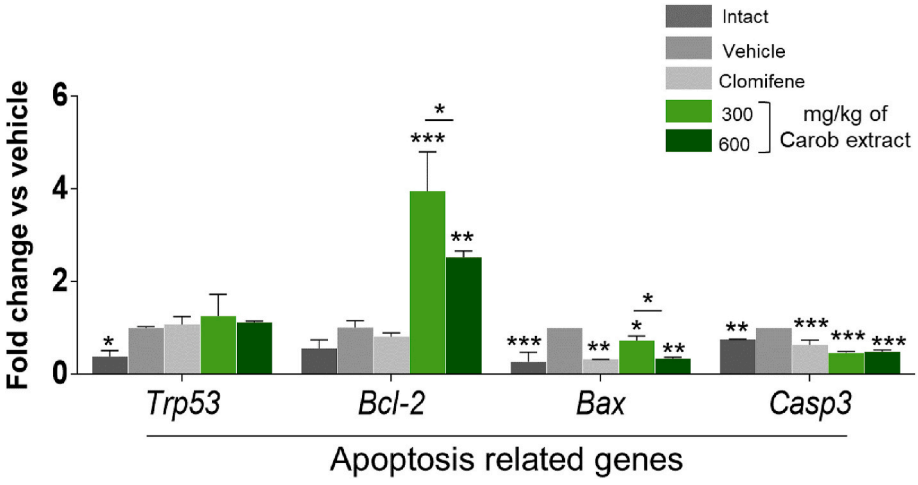

Fig. 8. Carob extract could improve the adverse effects of busulfan. Following the adverse effect of busulfan, *Bcl-2* (anti-apoptotic gene) had considerably elevated expression at the 300 mg/kg and 600 mg/kg doses of extract compared to the vehicle group ($P \leq 0.01$). As expected, the pro-apoptotic gene BCL2-associated X (*Bax*) significantly decreased with the 300 mg/kg and 600 mg/kg doses of carob in comparison with the vehicle group ($P < 0.05$). *Casp3,* a critical marker in the executive phase of apoptosis, significantly decreased in the 300 mg/kg and 600 mg/kg doses of carob in comparison with the vehicle group ($P \leq 0.0002$). Data for three independent experiments. Bars indicate mean ± SD. Based on assessment of data distribution, statistical significance was tested by one-way ANOVA with post-hoc Fisher's LSD test. *$P \leq 0.05$, **$P \leq 0.01$, ***$P \leq 0.001$.

spermatozoa. Our results supported the findings reported by Vafaei et al. where various sperm parameters considerably increased following carob administration in a busulfan treated infertile mouse model (Vafaei et al., 2018) and improved fertility in the experimental animal. However, the data they presented for sperm parameters was not strong, and they did not evaluate spermatogenesis related genes. Moreover, our results showed that carob helps to maintain DNA integrity as well as had antioxidant activity by decreased levels of H_2O_2 and O2•−.

In the present study, we found that both estradiol and testosterone levels significantly increased following carob administration. In male mice, deactivation of estrogen receptors or estrogen depletion reduces spermatogenesis and sperm production (Hauser et al., 2002). Simultaneous increase in both hormones following carob treatment may be a compensative response to decreased levels of these hormones after busulfan injection as it is in vehicle group. A limitation of our study is lack of hormone assessments at longer time after carob treatment to see whether hormonal levels will reach the normal level as it is in intact group.

Our study supplies the first insight into the gene expression patterns that underlie carob function.

The results of our study showed increased levels of the self-renewal and differentiation genes, as the key determinants in the spermatogenesis progress (Chen and Liu, 2015) in carob administrated testes. In line with our findings, it has been proven that Sertoli cells induce self-renewal in SSCs by secreting GDNF, which acts by binding to its receptor, *Gfr-α1* (Chen and Liu, 2015). In one study's result showed the importance of *Bcl-6b* for maintenance of SSCs self-renewal (Oatley et al., 2006). Also, *Utf-1* is a conserved molecule in undifferentiated spermatogonia that plays an important role in SSCs self-renewal, and in fetal and neonatal testicular gonocytes (Jung et al., 2014a). Thus, it seems that carob extract could promote self-renewal in these cells by inducing expressions of the GDNF pathway components (*Gfr-α1* and *Bcl6-b)* and SSC self-renewal gene (*Plzf* and *Utf-1)* expressions (Chen and Liu, 2015).

Our result showed significant increases in the genes involved in SSC differentiation (*Dazl*, *c-Kit*, *Ngn3*, *Stra8,* and *Smc1b)* following carob administration. According to previous studies, *Dazl* is expressed in differentiated spermatogonia and spermatocytes in the pachytene stage (Jung et al., 2014b). *c-Kit* expressed *Ngn3*, and it seems that *c-Kit* is involved in spermatogonia differentiation ergo, is a marker of differentiated spermatogonia type $A_{1\text{-}B}$ and plays a critical role in survival and proliferation (Qin et al., 2017). Overexpression of *Ngn3* induced spermatogonia cell differentiation and indirectly promoted *Stra8* and *c-Kit* expressions, which led to accelerated spermatogenesis and meiotic divisions (Tang et al., 2014). *Stra8* is expressed at the onset of meiosis in germ cells (Ma et al., 2018). *Smc1b* is expressed in spermatocytes during the prophase I stage of meiosis and it supports telomeres (Kleppe et al., 2017). Thus, it seems that carob extract promotes differentiation in these cells by activating the expressions of genes that play a role in spermatogonia cell differentiation. As a result, spermatogonia cells convert to their own differentiated lineage and advance to the spermatozoa stage. Notably, we observed that the highest dose of the carob extract induced spermatogonia proliferation and differentiation into spermatocytes followed by spermatocyte differentiation into spermatids and spermatozoa. *Dazl* expression increased in the 600 mg/kg dose in comparison with the 300 mg/kg dose, which showed a dose-dependent relationship in differentiating spermatogonia cells into spermatocytes and differentiation to spermatogonia lines. This finding was consistent with the increased *Dazl* expression pattern in cells that had reduced *c-Kit* expression (Zhang et al., 2011).

Chromatin compaction is a vital step during sperm maturation and fertilization ability (Manochantr et al., 2012). It plays a critical role in sperm head shape (Hammadeh et al., 2000) and is expected to impact sperm function. Protamine, Tnp1 and Tnp2 are involved in sperm chromatin compaction; histone substitution by Prm1 in testis tissue plays a vital role in the compaction of chromatin, which is required to maintain the quality of potent spermatozoa (Kempisty et al., 2007). *Prm1* as the most vital gene in spermatogenesis, is expressed in testis tissue, post-meiotic spermatids, and during the early stages of spermatogenesis that is along with Tnp1 and Tnp2, are involved in sperm production (Akmal et al., 2016). We could conclude that carob extract, by activating *Prm1*, *Tnp1*, and *Tnp2* gene expressions, promotes spermatozoa maturation during spermiogenesis and maintains their chromatin density. The results of our study show significant increases in the genes related to the spermatogenesis signaling pathways (GDNF, TGF-β, and BMP4) after carob extract administration. GDNF signaling pathway is involved in SSC self-renewal and differentiation (He et al., 2009). *Etv-5* and *Bcl-6b*, are two important components, which, is involved in SSCs self-renewal, and is required for their differentiation (He et al., 2009; Oatley et al., 2006). In our study, for the first time, we hypothesized that carob might promote self-renewal activity of SSCs via activation of the GDNF signaling pathway.

Our result confirmed that carob might promote the differentiation process in spermatogonia via activation of the TGF-β pathway (Fig. 9). The BMP4 pathway serves a crucial role in promoting germ cell development, spermatogenesis, and induction of differentiation in SSCs (Li et al., 2014). Likewise, BMP4 promotes DNA synthesis and proliferation of Sertoli cells via *Smad 1/5* expression. BMP4 regulates the synthesis of critical proteins for spermatogenesis by activating *Smad 1/5* (Hai et al., 2015; Li et al., 2014; Ni et al., 2019). We observed significant increases in the BMP4 signaling target genes: *Smad1*, *Smad5*, *BMP4*, *Id1-1,* and *Id2* following administration of the carob extract. For the first time, our study has concluded that carob promotes SSC self-renewal to maintain their pool via activation of the GDNF pathway and induces differentiation during the spermatogenesis process by activation of TGF-β and BMP4 (Fig. 9). This conclusion supported our results on the spermatogenesis genes, which confirmed upregulation of genes involved in both SSC self-renewal and differentiation. However, loss of function experiments should be conducted to further clarify the function of these pathways following carob administration.

Increased Sertoli cell-related genes following carob administration is consistent with increased spermatogenesis. Because Sertoli cell support spermatogonia development into spermatids (Fig. S5). Davidoff et al. have reported that *Nestin* gene expression increased during testis tissue growth and (Davidoff et al., 2004). Importantly, increased *Nestin* expression can differentiate the stem cell state of Leydig cells to mature steroid-secreting cells that can synthesize testosterone (Stanley et al., 2012). Thus, consistent with previous studies, the results of the present study demonstrated that the carob extract stimulated Leydig cell maturation via upregulation of *Nestin* in these cells and consequently increased testosterone levels. Carob extract also protects spermatogonial cells during spermatogenesis by maintaining the integrity of Sertoli cells (Fig. S5).

Our results suggest that carob promotes proliferation in the whole testis. Cell cycle-related genes are essential for germ cell growth and proliferation during all stages of spermatogenesis (Roy Choudhury et al., 2010). Expressions of *Cdk4*, *Cdk6*, *Ccnd1*, *Cdc25a*, and *c-Myc* genes, as activators of the cell cycle, significantly increased after administration of the carob extract. Moreover, we have observed significant decreases in the cell cycle inhibitor genes *P21*, *P57,* and *Pcna* after administration of carob. In addition, *Ki67* expression, as an important gene in cell proliferation, underwent a significant dose-dependent increase following carob consumption (Xu et al., 2016). As a result, the proliferation of spermatogonia increased in testicular tissue, which enabled the azoospermia mice to undergo additional spermatogenesis and produce more spermatozoa.

Our study suggests an anti-apoptotic role for the carob extract as revealed by increased level of anti-apoptotic gene (*Bcl-2*) in carob treated groups (Fig. 9).

5. Conclusion

Based on the findings of this study, carob extract induces

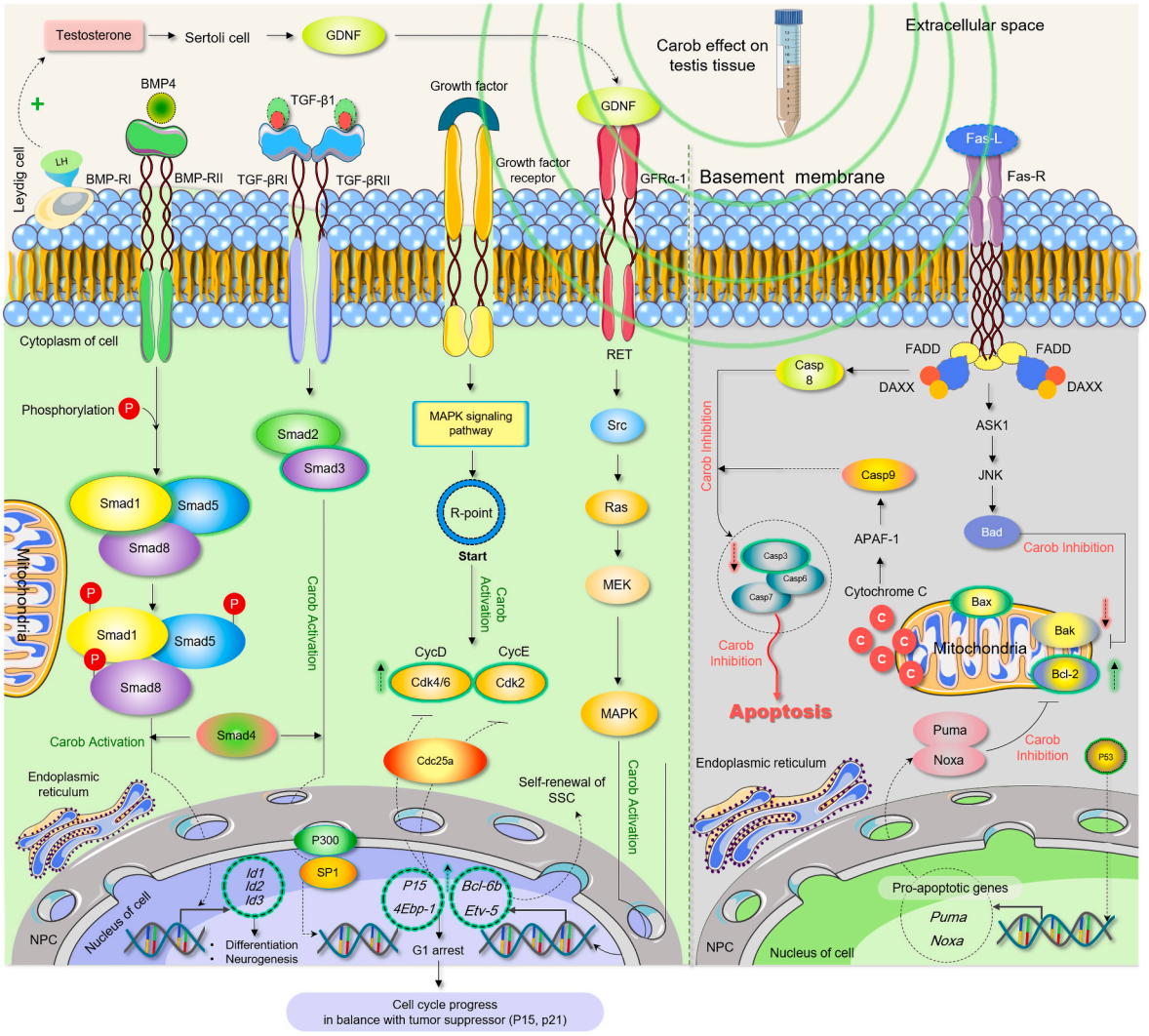

Fig. 9. Schematic presentation of carob extract effects on the expressions of target genes involved in spermatogenesis, including glial cell-derived neurotrophic factor (GDNF), transforming growth factor β (TGF-β), and bone morphogenetic protein 4 (BMP4) signaling pathways.

spermatogenesis in an infertile mouse model by affecting genes involved in spermatogenesis, activating the GDNF, TGF-β, and BMP4 signaling pathways and targeting the hormonal system. Our study revealed an anti-apoptotic role for carob extract in testes and activation of cell cycle regulating gene expressions. The efficacy of this herb in the infertile human testis has yet to be determined; thus, clinical trials should be conducted to evaluate the efficacy of carob administration for treating infertile azoospermia men.

Ethical statement

The animals were maintained according to the guidelines approved by the Royan Institutional Review Board and the Institutional Ethical Committee of Royan Institute (ethical code: IR.ACECR.ROYAN.REC.1397.008).

Authors' contributions

Z.G.: Collection and data assembly, data analysis and interpretation, manuscript writing. A.E.: Contributed to data collection. M.G.: Performed gene expression experiments for mice that received the carob extract. M.A.: Prepared the carob extract. M.A., J.Z., and M.K.: Performed the experiments and data analysis to prepare a metabolic profile of the extract. H.B.: Data analysis and interpretation, and manuscript writing. P.E. and F.E.: Study conception and design, data analysis and interpretation, manuscript proof, and administrative and financial support.

Funding

This study was supported by a grant from Royan Institute (grant no. 96000255) to F.E. and P.E.

CRediT authorship contribution statement

Zeynab Ghorbaninejad: Data Collection and assembly, data analysis and interpretation, manuscript writing. **Atiyeh Eghbali:** Contributed to data collection, , administrative and financial support. **Mahsa Ghorbaninejad:** Performed gene expression experiments. **Mahdi Ayyari:** Prepared the carob extract, Performed the experiments and data analysis to prepare a metabolic profile of the extract. **Jerzy Zuchowski:** Performed the experiments and data analysis to prepare a metabolic profile of the extract. **Mariusz Kowalczyk:** Performed the experiments and data analysis to prepare a metabolic profile of the extract. **Hossein Baharvand:** Data analysis and interpretation, and manuscript writing. **Poopak Eftekhari-Yazdi:** Performed the experiments and data analysis to prepare a metabolic profile of the extract. **Fereshteh Esfandiari:** Supervision, Writing – review & editing, Study conception and design,

data analysis and interpretation, Supervision, manuscript writing, review .

Declaration of competing interest

The authors declare that they do not have any conflicts of interest.

Data availability

Data will be made available on request.

Acknowledgements

We would like to express our appreciation to Dr. Rabientaj for her advice on determining the concentrations of the extract and Miss Forough Azam Sayahpour for her kind support during the gene expression experiments.

Appendix A. Supplementary data

Supplementary data to this article can be found online at https://doi.org/10.1016/j.jep.2022.115760.

References

Akmal, M., Widodo, M.A., Sumitro, S.B., Purnomo, B.B., 2016. The important role of protamine in spermatogenesis and quality of sperm: a mini review. Asian Pac. J. Reprod. 5 (5), 357–360.
Artimani, T., Amiri, I., Soleimani Asl, S., Saidijam, M., Hasanvand, D., Afshar, S., 2018. Amelioration of diabetes-induced testicular and sperm damage in rats by cerium oxide nanoparticle treatment. Andrologia 50 (9), e13089.
Ata, A., Yildiz-Gulay, O., Güngör, S., Balic, A., Gulay, M., 2018. The effect of carob (Ceratonia siliqua) bean extract on male New Zealand White rabbit semen. World Rabbit Sci. 26 (3), 209–215.
Babakhanzadeh, E., Nazari, M., Ghasemifar, S., Khodadadian, A., 2020. Some of the factors involved in male infertility: a prospective review. Int. J. Gen. Med. 13, 29–41.
Baker, K., Sabanegh Jr., E., 2013. Obstructive azoospermia: reconstructive techniques and results. Clinics 68, 61–73.
Berna, A., Pérez-Gago, M.B., Guardiola, V.G., Salazar, D., Mulet, A., 1997. Effect of temperature on isobutyric acid loss during roasting of carob kibble. J. Agric. Food Chem. 45 (10), 4084–4087.
Bucci, L.R., Meistrich, M.L., 1987. Effects of busulfan on murine spermatogenesis: cytotoxicity, sterility, sperm abnormalities, and dominant lethal mutations. Mutat. Res. Fund Mol. Mech. Mutagen 176 (2).
Chen, S.-R., Liu, Y.-X., 2015. Regulation of Spermatogonial Stem Cell Self-Renewal and Spermatocyte Meiosis by Sertoli Cell Signaling. Society for Reproduction and Fertility.
Chen, Z., Liu, M., Hu, J.-H., Gao, Y., Deng, C., Jiang, M.H., 2021. Substance P restores spermatogenesis in busulfan-treated mice: a new strategy for male infertility therapy. Biomed. Pharmacother. 133, 110868.
Cordeiro Jr., D.A., Costa, G.M., França, L.R., 2021. Testis structure, duration of spermatogenesis and daily sperm production in four wild cricetid rodent species (A. cursor, A. montensis, N. lasiurus, and O. nigripes). PLoS One 16 (5), e0251256.
Curtis, S.K., Amann, R., 1981. Testicular development and establishment of spermatogenesis in Holstein bulls. J. Anim. Sci. 53 (6), 1645–1657.
Davidoff, M.S., Middendorff, R., Enikolopov, G., Riethmacher, D., Holstein, A.F., Muller, D., 2004. Progenitor cells of the testosterone-producing Leydig cells revealed. J. Cell Biol. 167 (5), 935–944.
Deans, B.J., Skierka, B.E., Karagiannakis, B.W., Vuong, D., Lacey, E., Smith, J.A., Bissember, A.C., 2018. Siliquapyranone: a tannic acid tetrahydropyran-2-one isolated from the leaves of carob (Ceratonia siliqua) by pressurised hot water extraction. Aust. J. Chem. 71 (9), 702–707.
Esteves, S.C., Miyaoka, R., Orosz, J.E., Agarwal, A., 2013. An update on sperm retrieval techniques for azoospermic males. Clinics 68, 99–110.
Farag, M.A., El-Kersh, D.M., Ehrlich, A., Choucry, M.A., El-Seedi, H., Frolov, A., Wessjohann, L.A., 2019. Variation in Ceratonia siliqua pod metabolome in context of its different geographical origin, ripening stage and roasting process. Food Chem. 283, 675–687.
Faramarzi, A., Aghaz, F., Jahromi, M.G., Bakhtiari, M., Khazaei, M., 2019. Does supplementation of sperm freezing/thawing media with Ceratonia siliqua improve detrimental effect of cryopreservation on sperm parameters and chromatin quality in normozoospermic specimens? Cell Tissue Bank. 20 (3), 403–409.
Fernández, J.L., Muriel, L., Goyanes, V., Segrelles, E., Gosálvez, J., Enciso, M., LaFromboise, M., De Jonge, C., 2005. Simple determination of human sperm DNA fragmentation with an improved sperm chromatin dispersion test. Fertil. Steril. 84 (4), 833–842.
Ghaleno, L.R., Valojerdi, M.R., Janzamin, E., Chehrazi, M., Sharbatoghli, M., Yazdi, R.S., 2014. Evaluation of conventional semen parameters, intracellular reactive oxygen species, DNA fragmentation and dysfunction of mitochondrial membrane potential after semen preparation techniques: a flow cytometric study. Arch. Gynecol. Obstet. 289 (1), 173–180.
Ghasemi, M., Bahadori, M., Faghani, M., Nasiri, E., Soleimani Rad, J., 2009. Buserelin inhibits apoptosis in male germ cells induced by busulfan in mouse testis. J Iran Anat Sci 7, 45–54.
Gruner, O.C., 1930. The Canon of Medicine of Avicenna. AMS PRESS INC NEW YORK.
Hai, Y., Sun, M., Niu, M., Yuan, Q., Guo, Y., Li, Z., He, Z., 2015. BMP4 promotes human Sertoli cell proliferation via Smad1/5 and ID2/3 pathway and its abnormality is associated with azoospermia. Discov. Med. 19 (105), 311–325.
Hammadeh, M., Nkemayim, D., Rosenbaum, P., Schmidt, W., 2000. Sperm morphology and chromatin condensation before and after semen processing. Arch. Androl. 44 (3), 221–226.
Hauser, R., Botchan, A., Yogev, L., Gamzu, R., Yosef, D.B., Lessing, J., Amit, A., Yavetz, H., 2002. Probability of sperm detection in nonobstructive azoospermic men undergoing testicular sperm extraction procedures unrelated to clinical parameters. Arch. Androl. 48 (4), 301–305.
He, Z., Kokkinaki, M., Dym, M., 2009. Signaling molecules and pathways regulating the fate of spermatogonial stem cells. Microsc. Res. Tech. 72 (8), 586–595.
Henkel, R., Maaß, G., Bödeker, R.H., Scheibelhut, C., Stalf, T., Mehnert, C., Schuppe, H. C., Jung, A., Schill, W.B., 2005. Sperm function and assisted reproduction technology. Reprod. Med. Biol. 4 (1), 7–30.
Hosseinpour, E., Shahverdi, A., Parivar, K., Sedighi Gilani, M., Nasr-Esfahani, M., Salman Yazdi, R., Sharbatoghli, M., Tavalaee, M., Chehrazi, M., 2014. Sperm ubiquitination and DNA fragmentation in men with occupational exposure and varicocele. Andrologia 46 (4), 423–429.
Hossen, M.J., Uddin, M.B., Ahmed, S.S.U., Yu, Z.-L., Cho, J.Y., 2016. Traditional medicine/plants for the treatment of reproductive disorders in Asia Nations. Pak. Vet. J. 36 (2), 127–133.
Hu, X., Ding, Z., Hong, Z., Zou, Z., Feng, Y., Zhu, R., Ma, J., Ge, X., Li, C., Yao, B., 2018. Spermatogenesis improved by suppressing the high level of endogenous gonadotropins in idiopathic non-obstructive azoospermia: a case control pilot study. Reprod. Biol. Endocrinol. 16 (1), 1–10.
Isidori, A., Sansone, A., Gianfrilli, D., 2017. Hormonal Treatment of Male Infertility: Gonadotropins and beyond, Endocrinology of the Testis and Male Reproduction. Springer International Publishing Cham, pp. 1–20.
Jung, H., Roser, J.F., Yoon, M., 2014a. UTF1, a putative marker for spermatogonial stem cells in stallions. PLoS One 9 (10), e108825.
Jung, H., Song, H., Yoon, M., 2014b. Stage-dependent DAZL localization in stallion germ cells. Anim. Reprod. Sci. 147 (1–2), 32–38.
Jung, S.-W., Kim, H.-J., Lee, B.-H., Choi, S.-H., Kim, H.-S., Choi, Y.-K., Kim, J.Y., Kim, E.-S., Hwang, S.-H., Lim, K.Y., 2015. Effects of Korean Red Ginseng extract on busulfan-induced dysfunction of the male reproductive system. J. Ginseng. Res. 39 (3), 243–249.
Kempisty, B., Depa-Martynow, M., Lianeri, M., Jedrzejczak, P., Darul-Wasowicz, A., Jagodzinski, P.P., 2007. Evaluation of protamines 1 and 2 transcript contents in spermatozoa from asthenozoospermic men. Folia Histochem. Cytobiol. 45 (I), 109–113.
Kleppe, L., Edvardsen, R.B., Furmanek, T., Andersson, E., Juanchich, A., Wargelius, A., 2017. bmp15l, figla, smc1bl, and larp6l are preferentially expressed in germ cells in Atlantic salmon (Salmo salar L.). Mol. Reprod. Dev. 84 (1), 76–87.
Kovac, J.R., Smith, R.P., Cajipe, M., Lamb, D.J., Lipshultz, L.I., 2017. Men with a complete absence of normal sperm morphology exhibit high rates of success without assisted reproduction. Asian J. Androl. 19 (1), 39.
Kumar, R., 2013. Medical management of non-obstructive azoospermia. Clinics 68, 75–79.
Li, Y., Zhang, Y., Zhang, X., Sun, J., Hao, J., 2014. BMP4/Smad signaling pathway induces the differentiation of mouse spermatogonial stem cells via upregulation of Sohlh2. Anat. Rec. 297 (4), 749–757.
Ma, H.-T., Niu, C.-M., Xia, J., Shen, X.-Y., Xia, M.-M., Hu, Y.-Q., Zheng, Y., 2018. Stimulated by retinoic acid gene 8 (Stra8) plays important roles in many stages of spermatogenesis. Asian J. Androl. 20 (5), 479.
Manochantr, S., Chiamchanya, C., Sobhon, P., 2012. Relationship between chromatin condensation, DNA integrity and quality of ejaculated spermatozoa from infertile men. Andrologia 44 (3), 187–199.
MH, A.K., 1844. Makhzan-al-Advia (Persian). Tehran University of Medical Science, Tehran.
Mokhtari, M., Sharifi, E., Sh, A., 2012. The effects of hydro alcoholic extract of Ceratonia siliqua L. seeds on pituitary–testis hormones and spermatogenesis in rat. Adv. Environ. Biol. 2778–2784.
Molaie, S., Shahverdi, A., Sharafi, M., Shahhoseini, M., Rashki Ghaleno, L., Esmaeili, V., Abed-Heydari, E., Numan Bucak, M., Alizadeh, A., 2019. Dietary trans and saturated fatty acids effects on semen quality, hormonal levels and expression of genes related to steroid metabolism in mouse adipose tissue. Andrologia 51 (5), e13259.
Nair, A.B., Jacob, S., 2016. A simple practice guide for dose conversion between animals and human. J. Basic Clin. Pharm. 7 (2), 27.
Ni, F.-D., Hao, S.-L., Yang, W.-X., 2019. Multiple signaling pathways in Sertoli cells: recent findings in spermatogenesis. Cell Death Dis. 10 (8), 1–15.
Oatley, J.M., Avarbock, M.R., Telaranta, A.I., Fearon, D.T., Brinster, R.L., 2006. Identifying genes important for spermatogonial stem cell self-renewal and survival. Proc. Natl. Acad. Sci. USA 103 (25), 9524–9529.
Owis, A.I., El-Naggar, E.-M.B., 2016. Identification and quantification of the major constituents in Egyptian carob extract by liquid chromatography–electrospray ionization-tandem mass spectrometry. Phcog. Mag. 12 (Suppl. 1), S1.
Papagiannopoulos, M., Wollseifen, H.R., Mellenthin, A., Haber, B., Galensa, R., 2004. Identification and quantification of polyphenols in Carob Fruits (Ceratonia siliqua L.)

and derived products by HPLC-UV-ESI/MS n. J. Agric. Food Chem. 52 (12), 3784–3791.
Qin, Q., Liu, J., Ma, Y., Wang, Y., Zhang, F., Gao, S., Dong, L., 2017. Aberrant expressions of stem cell factor/c-KIT in rat testis with varicocele. J. Formos. Med. Assoc. 116 (7), 542–548.
Roy Choudhury, D., Small, C., Wang, Y., Mueller, P.R., Rebel, V.I., Griswold, M.D., McCarrey, J.R., 2010. Microarray-based analysis of cell-cycle gene expression during spermatogenesis in the mouse. Biol. Reprod. 83 (4), 663–675.
Sharma, S.S.a.A.K., 2017. Female anti-fertility screening of plants mucuna prurita, mesua ferrea and punica granatum on rat. Int. J. Pharmaceut. Chem. Res. 3 (3).
Sharma, S., Singh, M., Khatri, P., Sharma, A.K., 2016. PHARMACOGNOSTIC AND PRELIMINARY PHYTROCHEMICAL SCREENING OF PLANTS MUCUNA PRURITA. MESUA FERREA, PUNICA GRANATUM.
Stanley, E., Lin, C.-Y., Jin, S., Liu, J., Sottas, C.M., Ge, R., Zirkin, B.R., Chen, H., 2012. Identification, proliferation, and differentiation of adult Leydig stem cells. Endocrinology 153 (10), 5002–5010.
Stansbury, J., 2019. Herbal formulares for health professionals. Endocrinology 3.
Süntar, I., 2019. Importance of ethnopharmacological studies in drug discovery: role of medicinal plants. Phytochemistry Rev. 1–11.
Tang, F., Yao, X., Zhu, H., Mu, H., Niu, Z., Yu, M., Yang, C., Peng, S., Li, G., Hua, J., 2014. Expression pattern of Ngn3 in dairy goat testis and its function in promoting meiosis by upregulating Stra8. Cell Prolif 47 (1), 38–47.
Vafaei, A., Mohammadi, S., Fazel, A., Soukhtanloo, M., Mohammadipour, A., Beheshti, F., 2018. Effects of carob (Ceratonia siliqua) on sperm quality, testicular structure, testosterone level and oxidative stress in busulfan-induced infertile mice. Pharmaceut. Sci. 24 (2), 104–111.
Van der Horst, G., Maree, L., 2010. SpermBlue®: a new universal stain for human and animal sperm which is also amenable to automated sperm morphology analysis. Biotech. Histochem. 84 (6), 299–308.
Xu, H., Shen, L., Chen, X., Ding, Y., He, J., Zhu, J., Wang, Y., Liu, X., 2016. mTOR/P70S6K promotes spermatogonia proliferation and spermatogenesis in Sprague Dawley rats. Reprod. Biomed. Online 32 (2), 207–217.
Zhang, L., Tang, J., Haines, C.J., Feng, H., Lai, L., Teng, X., Han, Y., 2011. c-kit and its related genes in spermatogonial differentiation. Spermatogenesis 1 (3), 186–194.
Zheng, J., Lu, Y., Qu, X., Wang, P., Zhao, L., Gao, M., Shi, H., Jin, X., 2016. Decreased sperm motility retarded ICSI fertilization rate in severe oligozoospermia but good-quality embryo transfer had achieved the prospective clinical outcomes. PLoS One 11 (9), e0163524.
Zhu, Z.-J., Yang, S., Li, Z., 2015. Transcriptome research on spermatogenic molecular drive in mammals. Asian J. Androl. 17 (6), 961.
Ziarati, N., Topraggaleh, T.R., Rahimizadeh, P., Montazeri, L., Maroufizadeh, S., Gilani, M.A.S., Shahverdi, A., 2019. Micro-quantity straw as a carrier for cryopreservation of oligozoospermic semen samples: effects of storage times and cryoprotectant. Cryobiology 86, 65–70.